Graphical Abstract

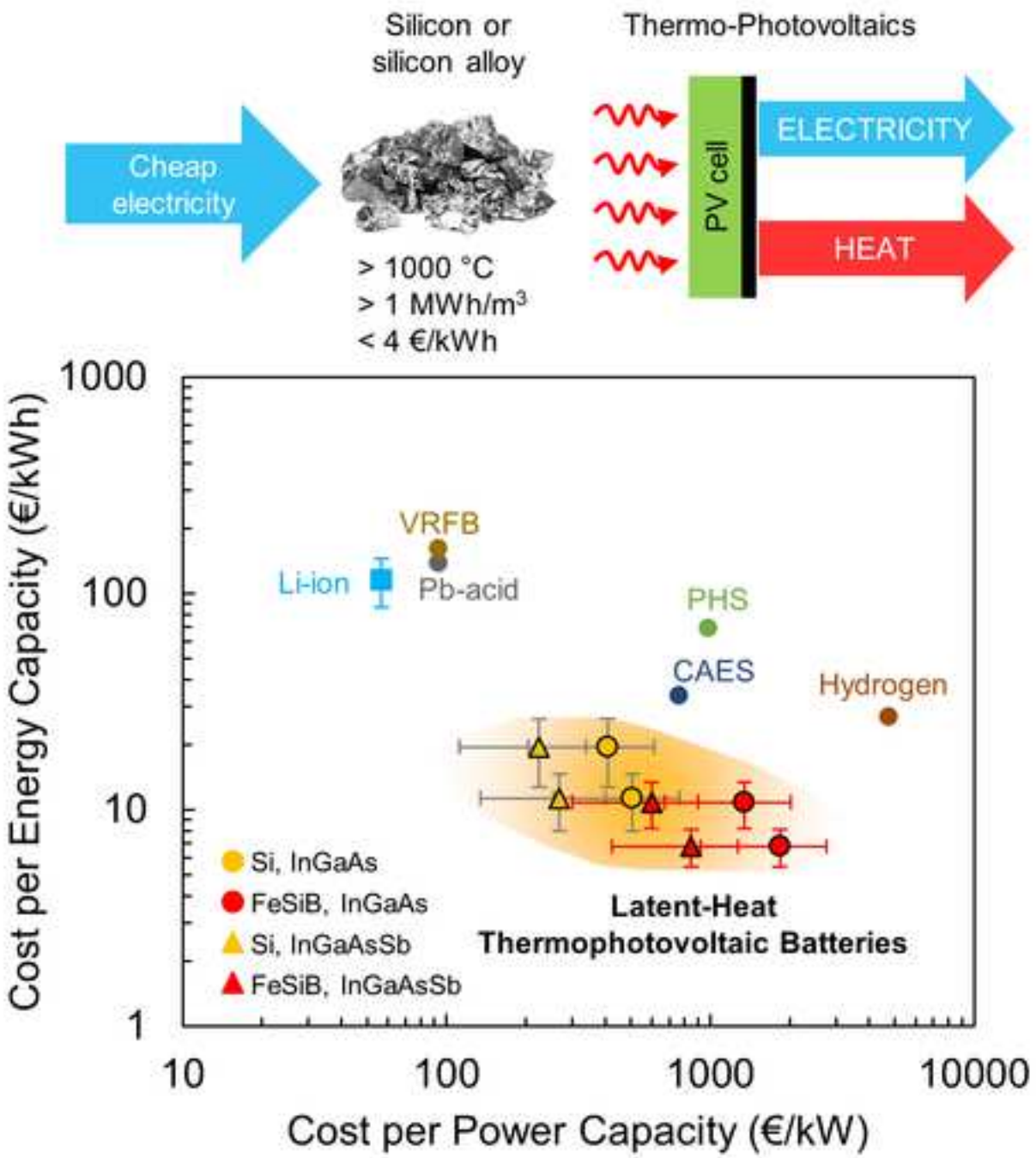

Latent Heat Thermophotovoltaic Batteries

Alejandro Datas[(1)(2)], Alicia López de Ceballos, Esther López, Alba Ramos[(+)], and Carlos del Cañizo

Instituto de Energía Solar – Universidad Politécnica de Madrid, Madrid, 28040, Spain

[(1)] corresponding author: a.datas@upm.es

[(2)] Lead contact

[(+)] currently at Universitat Politècnica de Catalunya, Jordi Girona 1-3, Barcelona 08034, Spain

Keywords: energy storage, thermophotovoltaics, power-to-heat-to-power, PHPS, electric thermal energy storage, ETES, thermal energy, high temperature, silicon, phase change materials, cogeneration, combined heat and power, CHP.

Summary

Latent heat thermophotovoltaic (LHTPV) batteries are power-to-heat-to-power storage systems in which electricity is employed to produce the solid-to-liquid transition in a phase change material (PCM), storing energy in the form of latent heat at very high temperatures (> 1000ºC). When needed, stored energy is released as thermal radiation, and converted back to electricity using thermophotovoltaics (TPV). In this study we discuss on the techno-economics of LHTPV systems, focusing on parameters like the round-trip efficiency, the energy-to-power ratio, the cost per energy and power capacities, and the levelized cost of storage. The relatively low TPV conversion efficiency (< 50 %) and the low cost of the PCMs (< 4 €/kWh) result in optimal designs with high energy-to-power ratios, fitting long duration storage (LDS) applications. The use of lower melting point PCMs, like FeSiB (1157 ºC), allows a significant reduction in the cost of thermal insulation, favouring their use in smaller scale applications. Shorter duration storage applications require lower cost per power capacity, which can be achieved by using higher melting point PCMs such as Si (1414 ºC), or higher round-trip conversion efficiency, which can be achieved through cogeneration, that is, combined heat and power (CHP) dispatchable generation. Results indicate that LHTPV systems can provide lower levelized cost of storage than Li-ion batteries in both LDS and CHP applications. Preliminary experimental results are provided to illustrate the real operation of a LHTPV system.

1 Introduction

Latent Heat Thermophotovoltaic (LHTPV) batteries are a kind of power-to-heat-to-power storage (PHPS) system [1–3], also named electro-thermal energy storage (ETES) [4] or thermal energy grid storage (TEGS) [5], that store electricity in the form of latent heat at very high temperatures (>1000ºC) and convert it back to electricity on demand using thermophotovoltaics (TPV) [6,7]. High melting temperature phase change materials (PCM), like silicon or silicon alloys [8], enable very dense energy storage (> 1 MWh/m^3) at very low cost (< 4 €/kWh) [1], and thus, they are very well indicated for long-duration energy storage applications. Long-duration energy storage systems [9] are characterized by having a high energy-to-power ratio and are intended to store the vast amounts of renewable electricity that would be lost otherwise. The price of this electricity (otherwise wasted) is very low, and the use of high-cost storage systems, like Li-ion batteries (> 80 €/kWh [10]), are not indicated in this case. On the contrary, systems with very low-cost per energy capacity (CPE) are preferable, even if they have lower round-trip conversion efficiencies. This is the case of Carnot-limited PHPS systems like LHTPV (in opposition to those that use a heat pump for heating [11]) whose round-trip electric-to-electric conversion efficiency is a fraction of the Carnot efficiency, i.e. $1 - T_c/T_h$, being T_c and T_h the temperature of the cold and hot reservoir, respectively. In addition to long-duration storage applications, PHPS (and LHTPV) systems are well indicated for dispatchable cogeneration from variable renewable energy sources [2]. The heat available in the system, either the one that is produced during the thermal-to-electric energy conversion or the one stored within the system, can be used to satisfy the heating demands in this case. The overall conversion efficiency is therefore increased, and the system can be profitable in a wider range of applications.

Several PHPS embodiments have been proposed in the recent years using a variety of thermal storage materials (stones, concrete, silicon, carbon, ceramics, etc.). Systems have been proposed in a very wide range of temperatures, ranging from ~ 500 ºC to over 1500 ºC, and use different kinds of thermal-to-electric energy converters [1,4]. PHPS systems that operate at very high temperatures (over ~ 1000 ºC) take advantage of the high enthalpy and high energy density of the stored heat [1,12]. Most commercial systems use heat engines that are based on well-established Rankine, Brayton, or Stirling thermodynamic cycles [13]. More innovative PHPS systems are based on TPV generators. Intended to operate at extreme temperatures (> 1000 ºC), TPV devices enable very dense, modular, silent, and low-cost power generation, ultimately resulting in very compact and scalable PHPS systems. PHPS systems based on TPV have been proposed using either solid- [1] or liquid- [5] sensible

heat, and latent heat [3] storage options. The main advantage of the latent heat options is the small temperature variation during the discharge (PCM solidification). This enables decoupling the energy storage and power generation capacities of the system. In sensible heat systems, high energy densities require very large variations of the storage media temperature, which imply a variable power generation capacity. As TPV generators require temperatures well over 1000 ºC to operate, most sensible heat options target extreme temperatures, well over 1500 ºC, to get a large temperature range at which the TPV generation is significant. Having such high temperatures in the charged state bring serious challenges on the thermal insulation. On the contrary, latent heat storage systems can be designed to provide an almost constant temperature during the discharge. In this way, a lower temperature can be targeted that relaxes the thermal insulation requirements without deteriorating the TPV power generation capacity. Therefore, the key of LHTPV systems is the selection of a PCM that enables high energy density and low cost (i.e., low thermal insulation requirements) along with reasonably high TPV power generation capacity. In this regard, silicon-based alloys enable very high energy densities (> 1 MWh/m^3) and very low costs (< 4 €/kWh) in a 'moderately high' temperature range (1157 – 1414 ºC) that mitigates the thermal insulation requirements but is still perfectly suited for TPV power generation. We will see that these features enable the development of very compact, silent, and scalable systems that could be used not only for long duration storage applications, but also for dispatchable cogeneration in space constrained locations such as buildings, factories, or districts. Furthermore, silicon and silicon alloys can be easily obtained from abundant raw or waste materials and eventually recycled after use, and therefore have the potential to minimize the environmental impact of the manufacturing of energy storage systems.

In this article we present a techno-economic assessment of LHTPV batteries, with an especial focus on their application for long duration energy storage and dispatchable cogeneration in a fully electrified building. Section 2 describes a LHTPV system configuration; section 3 provides a techno-economic assessment of LHTPV, and section 4 present preliminary experimental results of a LHTPV lab-scale test bed unit that can be used to test different materials and devices under real operation conditions.

2 LHTPV system

Figure 1 (a) shows a block diagram of a generic LHTPV system that includes electrical and thermal switches / regulators, a heating system, a thermally insulated heat store (including the PCM and the

thermally insulated container), and the TPV generator. Low-cost, high melting temperature and high latent heat PCMs, like silicon, iron, and silicon-iron-boron alloys (see **Table 1** and **Figure S1** in the **Supplemental Information**) are, in principle, interesting candidates for LHTPV applications. Silicon is a particularly interesting material due to its low cost and high energy density (both gravimetric and volumetric). However, volumetric expansion upon solidification might be an issue regarding thermal cycling reliability [14,15]. The recently proposed Fe-26Si-9B alloy (FeSiB for short) has a volumetric latent heat similar to that of pure silicon and negligible volume expansion upon solidification, allowing for a reliable melting / solidification cycling [16]. The lower gravimetric latent heat of FeSiB, which is attributed to the higher density of iron, is not a relevant issue for stationary applications. Moreover, FeSiB could be produced at low cost by using cheap raw and waste materials like silicon, scrap iron, and borosilicate glass. Furthermore, these materials have relatively high thermal conductivities that enable an efficient heat extraction, and can be contained (in liquid state) in carbon and silicon carbide crucibles [5,8]. For thermal insulation, a layered system that uses high-temperature and high-cost thermal insulation materials (TIM), like alumina fiber mat, for the inner side, and low-temperature and low-cost materials, like fumed silica board, for the outer side, are used to minimize the overall cost of the system [17] (**Table 1**). Electric heating can be accomplished using ohmic [18], induction [4], microwave [19], or arc systems [20], and electric switching / regulation can be accomplished by thyristor or IGBT blocks. Thermal switching can be performed by mechanical retracting or introducing the TPV generator in an enclosure within the system, thus, passing from dark to illuminated conditions.

Figure 2 shows a possible LHTPV embodiment that is based on the hollow cylindrical crucible units described elsewhere [3,21]. In this arrangement, the TPV generators can be mechanically retracted from the emitter, which is a cylindrical enclosure that is made in a crucible that contains the PCM. At the beginning of the discharge, the PCM is in the liquid state near its melting point. When the TPV generator is introduced in the enclosure, the PCM releases latent heat towards the emitter (the inner SiC crucible wall) and starts solidifying. During this process, a solid-liquid interface moves away from the emitter, creating a solid crust around the emitter that hinders heat transfer to the TPV generator. A temperature gradient, which increases over time, is established through the solid crust and the inner walls of the crucible that negatively impacts the TPV output power. In this regard, the advantage of this configuration is that the PCM cross-sectional area (perpendicular to the heat flux) diminishes in the direction of heat flux during the discharge, and thus, the heat flux density (in W/cm^2) is maximized at the emitter surface. This results in a small

heat transfer that ultimately results in a low temperature gradient through the PCM, subsequently enabling a more efficient thermal-to-electric energy conversion [21].

Figure 3 shows the average (solid lines) and the maximum/minimum (colored region) emitter temperatures during the discharge as a function of the discharge duration for two different system designs that have large (R_{cont}=34 cm) and small (R_{cont}=19 cm) crucible radius. Results are obtained using a slightly modified version of the quasi-1D heat transfer models described elsewhere [3] that assumes a perfectly adiabatic thermal insulation. This model calculates the temperature gradients in the PCM and the inner crucible walls during the solidification of the PCM. The discharge duration can be varied in this case through the size (the area) of the TPV generator that is introduced in the system, which determines the heat flow. Low temperature gradients in the PCM are expected for small TPV generators that are discharged slowly at a low-power rate. High temperature gradients are expected for large TPV generators that are discharged quickly at a high-power rate. Results in **Figure 3** illustrates that smaller container (R_{cont} = 19 cm) enables much lower temperature gradients, even at high power rates, at the expense of having a lower energy density, as there is large fraction of the volume dedicated to the container rather than the PCM itself. We will see that lower energy densities bring higher costs per energy capacity due to the need of higher amounts of thermal insulation materials. Therefore, a trade-off exists between the cost per power and the conversion efficiency (linked to the average temperature of discharge) and the cost per energy (linked to the energy density) that is determined by the crucible design and the storage duration.

3 Technoeconomics

The main technoeconomic parameters of this system (see **Figure 1**) are: (i) the energy capacity ($E = mL$), which is proportional to the total amount of PCM (m, in kg) and its latent heat of fusion (L, in kWh/kg); (ii) the cost per energy capacity (CPE, in €/kWh), which accounts for the cost of the PCM, its container, and the thermal insulation system; (iii) the charge and discharge durations at nominal power conditions ($t_c = E/Q_{in}$ and $t_d = E/Q_{out}$), which are determined by the energy-to-power ratios at the input and the output, respectively; (iv) the charge conversion efficiency ($\eta_c = Q_{in}/P_{in}$) and the cost per input power capacity (CPP_{in}, in €/kW_{el}), which are determined by both the electric switching/regulation and heating systems, and (v) the discharge electric conversion efficiency $\eta_d = P_{TPV}/Q_{out}$ and the cost per power capacity at the output (CPP_{out}, in €/kW_{el}), both determined by the TPV energy converter. The heat loss of the system can be accounted for in the overall input and output conversion efficiencies as $\eta_{in} = \eta_c/(1 + k_{loss}\, t_c/(t_d + t_c))$ and $\eta_{out} =$

$\eta_d(1 - k_{loss}\, t_d/(t_d + t_c))$, being k_{loss} the fraction of the total energy storage capacity (E) that is lost per cycle through the thermal insulation system. The levelized cost of electricity storage (LCOS) of the system (only accounting for the electricity output) can be formulated as a function of the parameters described above by neglecting the maintenance costs, and assuming a periodic cycling of the system that operates at nominal power conditions [1]:

$$LCOS = \frac{p_e}{\eta_{rt}} + \frac{1}{N_{cycl}}\left(\frac{CPP_{in}^*}{\eta_{rt} t_c} + \frac{CPE^*}{\eta_{out}} + \frac{CPP_{out}^*}{t_d}\right) \quad (1)$$

where $\eta_{rt} = \eta_{out}\eta_{in}$ is the round-trip conversion efficiency, p_e is the price of the energy input, $N_{cycl} = 8760/(t_d + t_c)$ is the number of cycles in one year, and CPE^*, CPP_{in}^*, and CPP_{out}^* are the annualized cost per power and energy capacities that are obtained from the initial capital expenditures CPE and CPP_i by $CPX_i^* = CPX_i \cdot r(1+r)^n/((1+r)^n - 1)$, being r the discount rate and n the lifetime of the installation (in years). LCOS is given in €/kWh-cycle and represents the average cost of the energy that is released by the system all through its lifetime. LCOS is the key figure of merit that should be minimized, and it increases with the cost per energy and power capacities and the price of input electricity but decreases with the conversion efficiency and the lifetime. Just by looking at this equation one can already understand that systems with high CPE require a high discharge conversion efficiency, and systems with high CPP_{out} require a long discharge duration. On the contrary, systems with very low CPE can tolerate lower discharge conversion efficiencies, and systems with low CPP_{out} can afford short duration discharge cycles.

3.1 Cost per energy capacity

The CPE of the system is determined by the PCM, its container and the thermal insulation. Thus, it can be calculated from the cost per volume (CPV, in €/l) and the volume (V) of each of these three elements in the system as $CPE = (CPV_{PCM}V_{PCM} + CPV_{cont}V_{cont} + CPV_{ins}V_{ins})/E$ being $E = \rho VL$ the total energy capacity of the system and ρ the gravimetric density of the PCM. The lower bound for CPE assumes negligible cost for the container and the thermal insulation, and it is solely determined by the cost and the energy density of the PCM. **Figure S1** in the **Supplemental Information** shows the volumetric energy density of several storage media, including PCMs (latent heat), as a function of the operation temperature (panel a), and their cost per volume (€/l) and their cost per energy capacity (€/kWh) (panel b) [1]. Low costs of the storage media, below 10 €/kWh, are possible with several sensible and latent heat options. However, to reach a low CPE the selected

media must not only be cheap but also ensure a low cost of the container and the thermal insulation subsystems. To that end, the storage media should also have a high energy density and a low operation temperature. The so-called 'solar salt' (40% KNO_3 + 60% $NaNO_3$) used in concentrated solar power plants have low cost (~ 7 €/kWh) at moderate temperatures (up to ~ 560 ºC), but the energy density is low (~ 0.1 MWh/m^3). Si and, potentially, FeSiB PCMs provide the highest volumetric energy density at the lowest cost (1.2 MWh/m^3 and 2.7 €/kWh), but their operation temperature is very high (1414 and 1157 ºC, respectively). In principle, it is not obvious whether the higher specific cost (in €/m^2) of the thermal insulation that is needed at higher temperatures is offset by the higher energy density and the lower cost of the storage media.

Panels (a) and (b) in **Figure 4** show the overall CPE of a LHTPV system as a function of the melting point and the latent heat of the PCM for different energy storage capacities (1 and 100 MWh, respectively). Two layers of thermal insulation material are considered: the outermost is a silica board that withstands up to 1000 ºC; the innermost is alumina fiber mat that withstands 1650 ºC [17] (see **Table 1**). The thickness of these two layers is calculated using a 1D heat transfer model to prevent exceeding 1000 ºC in the silica board and to obtain a certain amount of heat loss, which in the case of panels a-d of **Figure 4** is 5 %/day (i.e., 20 days of self-discharge duration). The number of crucibles is set to meet the energy storage capacity of the system in each case.

As expected, the lowest CPE are obtained by a hypothetical PCM with the lowest melting point and the highest latent heat (**Figure 4** a,b). Increasing the temperature implies the use of a thicker thermal insulation material, subsequently increasing the overall cost of the system. Exceeding 1000 ºC is particularly disadvantageous, as this is the temperature limit of fumed silica board, and the inner thermal insulation layer must incorporate the more expensive alumina fiber mat in this case. The impact of increasing temperature is particularly significant for systems with a small energy capacity (**Figure 4** a) and using a PCM with a low latent heat. On the contrary, the impact of increasing the temperature is negligible if the energy capacity of the system is high and the PCM has a high latent heat (**Figure 5**-b), as it is the case of Si and FeSiB PCMs. In other words, the use of Si or FeSiB PCMs is especially well indicated for large scale thermal energy storage. In this case, the amount of thermal insulation that is needed is very small if compared to the amount of thermal energy that is stored, and thus, a thermal insulation system with a higher specific cost (in €/m^2) is affordable. At smaller scales, larger amounts of thermal insulation materials are needed per stored energy capacity, and thus, reducing the specific cost of thermal insulation is important. In this

regard, the lower melting temperature of FeSiB (m.p. 1157 ºC) is very advantageous. The impact of scale on the CPE is further illustrated in **Figure 4** -c, which clearly shows that FeSiB PCM enables the lowest CPE at the smallest scales. **Figure 4** -d also shows that using fewer amounts of thermal insulation (i.e., using FeSiB PCM) results in a higher overall energy density. It should be noted that, under the assumptions of this study, PCMs with lower melting temperature (< 600 ºC) must exceed 400 kWh/m^3 at costs below 0.8 €/l to reach lower CPE than a system based on FeSiB. Besides, the selected PCM should have a high thermal conductivity. Otherwise, smaller containers with higher surface-to-volume ratios should be used for an efficient heat extraction, which would result in even higher CPEs and lower energy densities. These requirements are hardly attainable by existing PCMs in this temperature range.

In the most favorable scenario shown in panels c and d of **Figure 4** (FeSiB PCM, H = 1.5 m, and a 100 MWh system capacity), TIM accounts for only 22 % of the total CPE. However, this share increases to 40 % and 84 % if heat losses are reduced to 2.5 %/day and 0.5 %/day, respectively. **Figure S2** in the **Supplemental Information** shows the shares of the three main energy-related system components (PCM, crucible and thermal insulation) to the total CPE of the system for several configurations (energy capacity and heat loss). The general trend is that the share of thermal insulation on the total CPE decreases with the energy capacity and the heat loss. The higher the share of thermal insulation, the higher the total CPE and the lower the energy density. Panels e and f in **Figure 4** show the CPE and the energy density, respectively, as a function of the self-discharge duration for a very large (1 GWh) LHTPV system with crucible height values between 2 and 5 m, as represented by the lower and upper bounds of each colored band, respectively. Every self-discharge duration corresponds to an amount of heat loss, ranging from 10 %/h (10 h of self-discharge) to 0.24 %/day (10,000 h of self-discharge). The case of current state-of-the-art molten salt TES, with ~ 1 GWh of storage capacity, is indicated with an star (~ 0.36 %/day or ~ 7000 h self-discharge duration, and 0.08 MWh/m^3, obtained by assuming ΔT = 250 ºC and the tank dimensions indicated in references [22,23]). We see that, under the assumptions of this study, both Si- and FeSiB-based LHTPV systems can reach lower CPE (panel e) and higher energy density (panel f) than that of a two-tank molten salt system with the same energy capacity and heat loss (self-discharge duration). Enabling higher amounts of heat loss (reducing the self-discharge duration in **Figure 4**-e) comes with a reduction in CPE, as expected. This illustrates an existing tradeoff between cost and efficiency of the thermal insulation. We will see later that this trade-off results in an optimum amount of heat loss that minimizes the levelized cost of storage depending on the

application (i.e., storage duration). However, it should be noted that reducing the CPE by tolerating higher amounts of heat loss might not be possible for the two-tank molten salt system, as this may result in the freezing of the salt. On the contrary, LHTPV systems can accommodate a larger amount of heat loss without risking its operation. Thus, they are more flexible for finding an optimal balance between cost an efficiency of the thermal insulation, which is key for long duration storage applications, as it will be seen later.

Figure 4 - e,f also shows that reducing heat losses in a system based on FeSiB PCM has a lower impact on the CPE and the energy density than in a system based on higher temperature PCMs like Si or, especially, Fe. Again, this is because of the lower cost of the materials used for thermal insulation in a system based on FeSiB. Very low CPE (< 6 €/kWh) and high energy densities (> 520 kWh/m^3) are attainable for self-discharge durations up to ~ 1000 hours in a system of 1 GWh capacity that is based on Si PCM. Longer self-discharge durations, up to ~ 2300 hours, would be attainable in systems that are based on FeSiB at the same cost and similar energy density. Systems based in Fe would result in self-discharge durations of only 200 hours if they need to reach similar costs, and the energy density would drop to 270 kWh/m^3. Panels e and f in **Figure 4** also show that systems based on small crucibles (R_{cont} = 19 cm) have a higher CPE due to the lower energy density and the higher amount of thermal insulation material that is needed. This confirms the trade-off existing between CPP and CPE concerning the selection of the crucible design, as mentioned above (in connection with the results in **Figure 3**).

3.2 Cost per power capacity and conversion efficiency

The CPP and efficiency of the system is determined by the energy conversion processes, i.e., power-to-heat and heat-to-power (TPV generator). Thus, the overall CPP depends on each element's power capacity (P) and cost per nominal power (CPP): $CPP = CPP_{in}P_{in} + CPP_{out}P_{out}$. For an resistive heater, the CPP_{in} varies depending on the operation temperature [18,24,25], being around a 3 €/kW for the case of heating elements based on metallic alloys that operate at maximum temperatures around 1200 ºC, or ~ 20 €/kW for SiC heaters that operate at higher temperatures (up to ~ 1600ºC). Despite lower CPP_{in} are attainable at lower temperatures, this cost is very small if compared to the cost of the TPV generator (CPP_{out} = CPP_{TPV}), as will be seen below, so the selection of the heating elements will have a small impact on the overall cost of the system. This low cost of input power also enables very asymmetric charge / discharge durations, which might be advantageous to store the high peaks of power from variable renewable electricity sources. It is

worth noticing that concerns on the incorporation of thermal bridges, which could depend on the use of different kinds of heating elements, are not considered in this analysis. Thermal bridges are elements (e.g., resistors, holding structures) that have higher thermal conductivity than the surrounding materials, creating a path of least resistance for heat transfer, and could drastically deteriorate the thermal insulation of the system. Thermal bridges could be avoided using highly resistive heating elements that can operate at high voltages and low currents, or using other kinds of wireless heating process, like microwaves.

Figure 5 shows the TPV conversion efficiency (panel a) and the cost per power capacity (CPP_{TPV}) (panel b) as a function of emitter temperature for two kinds of TPV cells, i.e., InGaAs (bandgap of 0.75 eV) and InGaAsSb (bandgap of 0.53 eV). Results are obtained using a detailed balance model [26] that assume an internal luminescence efficiency of 84% (reported for InGaAs TPV cells [27]) and a cell temperature of 80ºC. In panel a, sub-bandgap reflectivities in the range of 90 to 98 % are considered, representing the lower and upper bounds of each colored band. The ideal case of TPV cells with perfect reflectors and an internal luminescence efficiency of 100% is also shown as a reference. In panel b, the TPV cost is assumed to be in the range of 1 – 3 €/cm^2 [28,29], representing the lower and upper bounds of each colored band, respectively. These costs are based on the analysis conducted for III-V semiconductor solar cells grown on Ge substrates that estimate a cell cost of less than 2 €/cm^2 [28], the substrate representing approximately 50% of it. This same study predicts that substrate re-use could drive the cell cost down to ~ 0.2 €/cm^2. Despite a higher cost is expected for InGaAs and InGaAsSb TPV cells that are based on today's more expensive InP and GaSb substrates, previous studies suggest that reaching cell costs of 1 €/cm^2 is doable in these materials in a high cumulative production scenario [29].

Results in **Figure 5** illustrate how CPP_{TPV} is drastically reduced at high temperatures due to the higher electrical power density that pays off the cost of the TPV converter. Assuming identical costs per unit of area for both InGaAs and InGaAsSb devices, the higher power density of InGaAsSb enables lower CPP_{TPV}, especially at low emitter temperatures. Thus, InGaAsSb TPV cells are especially indicated for LHTPV systems that use 'low' temperature PCMs, like FeSiB. Otherwise, InGaAs TPV cells might be preferable due to the higher conversion efficiency potential at higher temperatures. As explained elsewhere, TPV conversion efficiency strongly depends on the photon recycling efficiency [6,30]. Back-surface reflectors (BSR) implemented on InGaAs TPV cells have recently demonstrated sub-bandgap reflectivities over 95 % and TPV cell conversion efficiencies of

~ 30 % [27,31]. InGaAsSb cells are less sensitive to photon recycling losses, as observed in the narrower band of InGaAsSb efficiencies plotted in panel (a) but have a lower upper bound for the conversion efficiency, especially at very high emitter temperatures. Due to the higher photogenerated current density, InGaAsSb cells are also more sensitive to ohmic losses, as illustrated by dashed lines in **Figure 6**. However, ohmic losses might not be as relevant for 'low' temperature LHTPV applications, where the use of InGaAsSb cells is more indicated.

When incorporated in a LHTPV system like the one shown in **Figure 2**, the emitter temperature will change over the discharge time, as illustrated in **Figure 3**, causing a dependence of CPP on the storage duration. Because more pronounced temperature variations are expected in systems with large radius PCM containers and high-power outputs, i.e., short discharge durations, the average CPP of TPV will be higher in this case. **Figure 6** captures this dependence by showing the CPP of a TPV generator for two kinds of LHTPV systems with R_{cont} = 34 cm (solid lines) and R_{cont} = 19 cm (dashed lines) and using two different PCMs: Si in panel (a) and FeSiB in panel (b). CPP is calculated considering the average discharge power, obtained as the total delivered electricity divided by the total discharge duration. A BSR reflectivity of 95 % is considered in these calculations, and the uncertainty for the cost per area of TPV generator (1 – 3 €/cm^2) is illustrated by the colored regions, as in **Figure 5**. The figure shows that smaller containers (R_{cont} = 19 cm) result in lower CPP for a broader range of storage durations for both Si and FeSiB-based systems, as expected. Besides, higher CPPs are obtained in systems using FeSiB PCM due to its lower melting temperature. Therefore, long discharge times (low power outputs) and the use of smaller containers (R_{cont} = 19 cm) is especially indicated in this case to minimize the temperature gradients in the PCM, and thus, minimize the CPP.

3.3 LHTPV applications

The application of any storage technology is determined by, at least, the following three figures of merit: the round-trip efficiency, the cost per energy capacity (CPE), and the cost per power capacity (CPP). As explained elsewhere [9,32], high efficiency and low CPP are important for short duration storage applications, whereas low CPE is key for long duration storage applications. **Figure 7** shows the CPE and CPP of different configurations of a LHTPV system, all of them having 100 MWh capacity, 50 h of storage duration (impacting on the CPP, as shown in **Figure 6**), and 1000 h of self-discharge duration (i.e., heat loss of 2.4 %/day). Cost estimates for other storage technologies (Li-ion, Pb-acid, Vanadium redox flow batteries, pumped hydroelectric, compressed

air energy storage, and hydrogen) are also shown as a reference [10,32]. A wide range of CPE values, starting at ~ 6 €/kWh, are possible for LHTPV depending on the choice of PCM (Si or FeSiB) and the container dimensions (H= 1 to 2 m, R_{cont} = 19 or 34 cm). Also, a wide range of CPP values, starting at ~ 100 €/kW_{el}, are possible depending on the type of TPV generator (InGaAs or InGaAsSb), their cost (in €/cm^2), the melting point of the PCM, and to a lesser extent, the PCM container radius (R_{cont} = 19 or 34 cm). In general, LHTPV systems can provide lower CPE than other existing technologies, especially than electrochemical batteries, which makes them appealing for long duration storage applications. On the other hand, LHTPV systems have a relatively high CPP (and low conversion efficiency), which is disadvantageous for short duration storage applications. A general trend is observed that FeSiB-based systems provide a lower CPE and higher CPP than those based on pure Si. This is a direct consequence of the lower melting point of FeSiB that led to lower thermal insulation requirements (lower CPE) and lower TPV generated power density (higher CPP). This already suggests that systems based on FeSiB PCM are better suited for longer duration storage applications, whereas Si-based LHTPV systems will perform better at shorter durations.

3.3.1 Long duration storage

As indicated above, the very low CPE is the major advantage of LHTPV if compared to other storage options. On the contrary, the main drawbacks are the low efficiency and the high CPP. This makes LHTPV well indicated for long duration storage (large energy-to-power ratio) applications, where having low cost per energy capacity is more important than anything else [9]. Panels a to f in **Figure 8** show the relative difference in LCOS between LHTPV and Li-ion batteries having an energy capacity of 100 MWh, and assuming their most favorable cost estimates (see figure caption). Relative difference in LCOS is shown as a function of the TPV efficiency, the heat loss (panels a to d) and the half-cycle storage duration (panels e and f) for LHTPV systems based on Si (panels a, c, e) and FeSiB (panels b, d, f). Remarkably, these figures show that there exists a minimum value of the TPV efficiency, depending on the storage duration and the heat loss, above which LHTPV provides lower LCOS than Li-ion batteries (red colored regions). This breakeven TPV efficiency is shown as a function of the storage duration and the energy storage capacity in panels a-d in **Figure 9** for different system configurations and TPV cell cost assumptions.

The breakeven TPV conversion efficiency is minimized at a certain amount of heat loss (panels a – d in **Figure 8**) that represents the fulfilment of a tradeoff between cost and efficiency of thermal

insulation. Such optimal amount of heat loss (in %/day) slightly decreases with the storage duration, ranging from 3.6 %/day (at 10 h half-cycle duration) to 2.9 %/day (at 100 h half-cycle duration) for the Si-based system (panels a and c), and from 2.2 %/day (at 10 h half-cycle duration) to 1.9 %/day (at 100 h half-cycle duration) for a system based on FeSiB PCMs (panels b and d). This is understandable, as more efficient thermal insulation system is needed when energy must be stored over longer periods. However, despite of the better thermal insulation, the total amount of losses (in %/cycle) significantly increases with the storage duration, being in the range of 16 and 24 %/cycle for FeSiB and Si PCMs, respectively (for the case represented in panels c and d). This shows that heat losses are more relevant at longer durations, and thus, the use of FeSiB is very advantageous in this case, enabling a reduction of up to ~ 8 % (absolute) in the total heat loss (for a system of 100 MWh energy capacity). This lower heat loss may counterbalance the lower TPV conversion efficiency that is expected in FeSiB-based LHTPV systems (**Figure 5**), and thus, the overall round-trip conversion efficiency could become comparable or even higher than that of Si-based systems. Remarkably, the breakeven TPV conversion efficiency decreases with the storage duration, as illustrated in panels e and f of **Figure 8**. Breakeven efficiencies lower than 20% are possible at very long durations, whereas very high (unattainable in practice) efficiencies of over 50 % are required at relatively short durations of around 10 hours.

Besides of the storage duration, the breakeven TPV conversion efficiency also depends on the energy capacity, as illustrated in panels a-d in **Figure 9** for a LHTPV systems with an optimized amount of heat loss. The optimal values for the heat loss and the crucible height, along with the resultant CPE that are obtained for this figure are shown in **Figure S3** of the **Supplemental Information**. Most favorable conditions for LHTPV are obtained at long durations and large energy capacities (panels a-d in **Figure 9**), where breakeven efficiencies are lower than 20 % regardless of the used PCM and the TPV cell type and cost. This is attributed to the very low CPE that is attainable by LHTPV at large scales, which is particularly important for long storage duration applications. On the other hand, very high breakeven efficiencies are obtained for short storage durations, regardless of the energy capacity, and especially if the cost of TPV is high. The higher efficiency and lower CPP of Li-ion batteries makes them preferable in this case, despite of the lower CPE of LHTPV. For a given energy capacity, increasing the storage duration generally brings a reduction in the breakeven efficiency. Only at small energy capacities, a slight increment is observed for very long storage durations (especially observed in panels a and c of **Figure 9**). This is attributed to the higher amounts of thermal insulation that are needed in this case (see **Figure S2** in

the **Supplemental Information**), which result in a higher CPE that needs to be counterbalanced by a higher TPV conversion efficiency. This effect is less noticeable in the case of using FeSiB (panels b and d) due to the lower requirements of thermal insulation. In fact, the main advantage of FeSiB-based systems occurs at small scales and long storage durations (top-left corner in all panels of **Figure 9**), where the breakeven TPV efficiencies (~ 30 %) are significantly lower than that of Si-based systems (> 40 %). On the contrary, Si-based systems are favored over FeSiB-systems at shorter storage durations (bottom part in all panels of **Figure 9**), where a higher amount of heat loss becomes affordable and the benefit of having a lower CPP is more noticeable. This is better illustrated in panels e and f in **Figure 9**, which show the relative difference in TPV breakeven efficiency between Si- and FeSiB-based LHTPV systems that use low cost (1 €/cm^2) InGaAsSb TPV cells (panel e) and high-cost (3 €/cm^2) InGaAs TPV cells (panel f), representing the best- and worst-case scenarios for the cost of TPV, as illustrated in **Figure 6**. These panels show that increasing the cost of TPV favors the use of Si over FeSiB in a broader range of applications, i.e., storage capacity and duration. On the contrary, the use of FeSiB is favored when the cost of TPV power is low, especially at small scales. Therefore, a Si-based system may be preferable in a scenario that very low bandgap TPV cells (like InGaAsSb) could not be manufactured with good performance and low cost. However, the benefits of using LHTPV over Li-ion would be limited to very long durations and very large storage capacities in this case.

3.3.2 Dispatchable cogeneration

The main two reasons why LHTPV systems cannot beat Li-ion batteries for short storage durations are the high CPP and the low conversion efficiency. A way to circumvent this limitation is to deliver the heat that is generated in TPV cells (typically at temperatures lower than ~ 70ºC) to satisfy heating demands, and thus, obtain some economical value from it. **Figure 10** shows two possible system configurations for the integration of energy storage in a cogeneration solution (combined heat and power) of a fully electrified building. The building comprises a solar-PV installation and uses the electricity from the grid as backup. Panel a show a system based on Li-ion batteries, whereas panel b shows a system based on LHTPV. Both use an electric boiler with an integrated hot water storage tank as an additional buffer for delivering the heating demands (hot water and space heating). The LHTPV unit delivers heat, not only from the cooling of the cells, but also directly from the PCM. This is a preferred alternative to use the electricity from the grid when the heating demand cannot be satisfied by other means. Both systems have been analyzed following a similar approach than in [2] (where a generic PHPS system is compared with a baseline scenario

that consumes natural gas and grid electricity), assuming simplified models for each component of the system and a relatively simple control strategy. Details on the model are provided in the **Supplemental Information**. The techno-economic parameters that, otherwise indicated, are fixed, or optimized during the simulations are show in **Table 3**. Like in our previous work [2], the hourly energy demands of a small residential building in Madrid have been simulated using Energy Plus® [33], resulting in an annual energy consumption of 19.5 MWh, being 3.9 MWh electricity (from which 1.1 MWh are consumed by the air conditioner) and 15.6 MWh heat (14.2 MWh for space heating and 1.4 MWh for domestic hot water). The hourly PV electrical power generation per kW of installed PV capacity is calculated by means of PVsyst® assuming an ideal tilt of the panels [34]. To consider different building sizes, these hourly energy demands are multiplied by a scale factor. Despite this approach might not accurately provide the actual energy demand of a large building, it will be useful to illustrate the scaling effects of LHTPV systems. The above methodology has been applied to different configurations of buildings of different sizes, heat consumption, and grid electricity prices with hourly discrimination, to corroborate that the following qualitative results and conclusions are general and valid, even though the quantitative analysis could change depending on the particularities of each application.

Figure 11 (panels a and b) show the levelized cost of energy (LCOE, in €/kWh) and the total energy density (in kWh/m^3) of the two systems illustrated in **Figure 10** as a function of the yearly energy demand, including two kinds of LHTPV systems that are based on InGaAsSb TPV cells and use either Si or FeSiB PCMs. The LCOE has a similar definition than the LCOS (see **Supplemental Information**) but referring to the average cost of the final consumed energy (heat and electricity) along the entire lifetime of the installation, and it includes both the initial capital expenditures of all components in the system and the cost of the electricity that is purchased from the grid. Any other maintenance costs (e.g., replacement of units) are neglected. The total energy density is defined as the total storage energy capacity of the installation, including the battery (either Li-ion or LHTPV) and the hot water store, divided by the total volume occupied by those components. Each colored band represent the values obtained within each technology' margin of confidence for their cost (see figure caption). The system has been optimized (see optimized parameters listed in **Table 3**) at each point targeting the minimum LCOE for each solution. **Figure S4** in the **Supplemental Information** shows the values obtained for all the optimized parameters that are listed in **Table 3**, i.e., the battery energy storage capacity, the battery output and input power capacity, the PV installed power

capacity, the hot water storage capacity, and the optimal crucible height and heat loss of the LHTPV battery.

Panel (a) in **Figure 11** shows that scaling up LHTPV systems enables a reduction in the LCOE, whereas Li-ion batteries produce a constant LCOE, independently of the scale. This is a direct consequence of the significant reduction of the CPE and the heat loss of the LHTPV systems at large scales. If the yearly energy demand is increased from 0.1 to 100 GWh/year in a Si-based LHTPV system, the optimal LHTPV energy capacity increases from ~ 180 kWh to 800 MWh, the CPE reduces from 40 €/kWh to 5.4 €/kWh and the optimal heat loss reduces from 20 %/day to 0.9 %/day. In a FeSiB-based system, the same tendency is observed but with lower values of CPE (from 18 €/kWh to 4.7 €/kWh) and heat loss (from 8 %/day to 0.5 %/day). At small scales, the cost of thermal insulation is significant, and thus, the optimal amount of losses is relatively high. This results in lower overall conversion efficiencies, higher costs per energy capacity, and ultimately, higher LCOE. The slightly lower LCOE obtained with Si-based systems at large scales is explained by the lower cost per power of the TPV generator, which goes from 362 – 1163 €/kW (at 0.1 GWh/year) to 173 – 444 €/kW (at 100 GWh/year), whereas for the FeSiB system it goes from 601 – 1273 €/kW (at 0.1 GWh/year) to 425 – 1075 €/kW (at 100 GWh/year). This indicates that, to obtain a lower LCOE in this application, having a low cost per power (Si-based systems) is more important than having a low cost per energy (FeSiB-based systems). This is understandable, as the average half-period of PV generation and energy consumption is relatively low in this case (~ 12 hours), and this requires a relatively low energy-to-power ratio. Indeed, the reduction in the cost per power at large scales is also explained by the increment in the energy-to-power ratio, which goes from 5 – 7 hours to 23 – 33 hours in the Si system, and from 18 – 40 hours to 40 – 70 hours in the FeSiB system. A large energy-to-power ratio enables a slow discharge process and a higher average emitter temperature that ultimately results in a lower cost of power capacity (**Figure 6**). The increment in the energy-to-power ratio is also explained by the fact that, at large scales, a large fraction of the LHTPV storage capacity is dedicated to store the heat that will be eventually used to satisfy the heating demands. At small scales, the large amount of heat that is lost in the LHTPV system prevents its use for this purpose, favoring the use of the hot water tanks, as it will be explained below.

Besides of the lower LCOE at large scales, the main advantage of LHTPV over Li-ion is the much higher overall energy density (**Figure 11**, panel b). A fully electrified system that is based on Li-ion

batteries will store large amounts of PV electricity in the form of hot water to eventually satisfy the heating demands. The low energy density of the hot water stores (46.5 kWh/m^3 for a temperature difference of 40ºC) results in a very low overall energy density. Most of the volume is dedicated to hot water stores in this case (~ 10,500 m^3 for 100 GWh/year, storing ~ 488 MWh of thermal energy), and the Li-ion batteries (assumed to have an energy density of 400 kWh/m^3) only represent a small fraction of the total volume (~ 164 m^3 for 100 GWh/year, storing ~ 66 MWh of electricity). On the contrary, a LHTPV system can store heat at much higher energy densities (up to ~ 600 kWh/m^3 at 100 GWh/year). Consequently, hot water stores are barely needed, and the overall energy density is significantly increased. Most of the volume is dedicated to the LHTPV system in this case (1300 – 1850 m^3 at 100 GWh/year, storing a thermal energy capacity of 0.7 – 1.1 GWh), and the hot water tanks represent a small fraction of the total system volume (130 – 180 m^3 at 100 GWh/year, storing 6 – 8 MWh of thermal energy), and are only used to store the heat coming from the cooling of the TPV cells.

Therefore, a key difference between LHTPV and Li-ion batteries in these applications regards the way of storing the surpluses of PV electricity for delivering the heating demand. In LHTPV systems, these surpluses are stored at high energy density in the LHTPV battery, which is oversized to deliver this additional heating demand. In the case of Li-ion batteries, these surpluses must be stored at low energy density in separate hot water tanks, which occupy a very large volume. The high amount of heat losses that exist in LHTPV systems at small scales favors the use of hot water tanks, and this explains the lower overall energy density of LHTPV-based systems that is obtained in this case. It should be noted that Li-ion batteries could be hybridized with other more efficient heating systems (e.g., heat pumps) and high energy density heat stores (e.g., low temperature PCM) to result in a more efficient and economical solution. The analysis of all these possible scenarios is outside the scope of this study and should be analyzed in future works.

The main difference between Si and FeSiB systems that is observed in **Figure 11** (panels a and b) is the scale at which LHTPV starts having a clear advantage over Li-ion. Despite Si-based systems provide slightly lower LCOE at large scales, FeSiB-based LHTPV systems become advantageous (i.e., provide lower LCOE and higher energy densities than systems based on Li-ion batteries) at smaller scales. Like in the previous section, this is linked to the lower cost per energy capacity that is attainable at smaller scales (**Figure 4**-a) due to the lower melting temperature of the FeSiB PCM that allows for a more efficient and cost-effective thermal insulation. **Figure 11** (panel c) shows the

LCOE for the best-case scenarios of both Li-ion and FeSiB-LHTPV batteries as a function of the yearly energy consumption for different costs of the PV installation, ranging from 600 €/kW to 2000 €/kW and for two cases of LHTPV systems: with an optimized crucible height (solid red lines) and a fixed crucible height of 1.5 m (dashed red lines). These figures show that the scale at which the LHTPV systems outperforms Li-ion batteries increases with the price of PV. This is also the case for the reduction in LCOE that can be obtained at large scales with LHTPV. Therefore, large scales and low PV prices favor the use of LHTPV systems over Li-ion batteries. As lower PV prices are attainable in large-scale installations, this reinforces the conclusion that self-consumption cogeneration solutions based on LHTPV should target very large-scale applications. Moreover, at large scale applications, a dedicated building is probably needed for the LHTPV system, which enables the use of tall crucibles (e.g., over 1.5 m), ultimately resulting in even lower LCOE.

Figure 12 shows the LCOE of a LHTPV system optimized at a yearly energy demand of 2 GWh/year, as a function of the TPV conversion efficiency. The optimal size of the LHTPV system ranges from 12 – 15 MWh (for Si systems) to 13 – 15 MWh (for FeSiB systems) and the optimal heat loss from ~ 4 %/day (for Si systems) to ~ 2.5 %/day (for FeSiB systems), independently of the TPV efficiency. The optimal size of the PV installation is ~ 2 MW, also independently of the type of LHTPV system and TPV conversion efficiency. This figure illustrates that a system based on LHTPV can get lower LCOE than those based on Li-ion batteries at a reasonably low TPV conversion efficiency of just over ~ 20 %, which is attainable with current existing technologies. Moreover, the increase in the conversion efficiency over ~ 40 % does not bring a very significant advantage. This is explained by the lower amount of heat that is obtained from the cooling of the cells in this case, which makes necessary to generate this heat by other means. If LHTPV only supplied electricity, one could expect the optimal energy and power capacities of the LHTPV and PV systems to decrease with the TPV conversion efficiency [35]. A clear advantage could be expected by increasing the TPV conversion efficiency in this case. However, if LHTPV supplies both heat and electricity in a fully electrified cogeneration application where the heating needs must be satisfied with electricity, either coming from the PV installation or from the grid, the PV and LHTPV installations still need to be sized to deliver the heating needs. This precludes a very significant advantage by increasing the TPV conversion efficiency over ~ 40 %. Increasing the TPV efficiency mostly impacts on the electricity consumption, which represents only 20 % of the total energy demand in this case, and thus, a relatively low TPV conversion efficiency is enough to have a significant impact on reducing the LCOE. The optimal size of the TPV generator that is obtained

at 40 % TPV conversion efficiency (e.g., 250 kW_{el} for the best-case scenario of a Si-based system) barely increases at higher efficiencies (e.g., 260 kW_{el} at 80 %), preventing a more significant advantage.

It worth noticing that the simulations shown in this section require a very large PV installation (e.g., from 1 to 10 MW for a yearly energy demand from 1 to 10 GWh and a PV cost of 900 €/kW). A large PV installation is needed to minimize the LCOE, i.e., avoid the use of electricity from the grid, due to the assumption of a constant price of grid electricity. In this case, the battery is only charged using electricity from the PV installation. On the contrary, if we assume hourly discrimination for the price of grid electricity, the battery could be charged with grid electricity during the valley periods, and thus, the required PV installation would be smaller. Analyzing this and other possible scenarios is out of the scope of this article and should be studied in future works.

4 An experimental test bed unit

An experimental LHTPV test-bed unit has been fabricated in the frame of the EU-funded AMADEUS project [36]. The system was designed for crucibles with an inverse truncated cone geometry, following previous designs intended for concentrated solar applications [21,37–39]. Like the hollow cylindrical configuration described in the previous sections, the inverse truncated cone geometry has a cross-sectional area (perpendicular to the heat flux) that diminishes in the direction of heat flux. This makes heat flux density (in W/m^2) to increase towards the TPV emitter; thus, minimizing the temperature gradient in the PCM during the solidification process. The fabricated system integrates a graphite heater to heat up the crucible from above by thermal radiation. The crucible has 0.63 liters of volume capacity, and it is thermally insulated from the environment by means of a ~ 25 cm cover of graphite fiber mat [17]. The TPV cell is mounted in a copper water cooled plate and faces the bottom of the crucible, and it produces electricity from the thermal radiation originating in the crucible walls. The purpose of this system is to be a test bed for the characterization of materials and devices that will be eventually used to develop optimized LHTPV systems.

Figure 13 shows preliminary results of the characterizations conducted with this system. Panel a shows the short-circuit current and the complete I-V characteristics (inset) of a 1.48 cm^2 GaSb TPV cell (from JX Crystals) as a function of the crucible temperature. Panel b shows the produced TPV power density as a function of the crucible temperature along with the projections made with a TPV

cell model that is based in detailed balance calculations [26]. A maximum power density of 478 mW/cm^2 has been measured at the maximum crucible temperature of 1030ºC, which is 59% of the theoretical maximum of 808 mW/cm^2 (assuming an ideal GaSb cell, unity view factor, and a crucible emissivity of 0.81). The highest TPV cell temperature is 37 ºC and it corresponds to the highest crucible temperature (1030 ºC). **Figure S5** in the **Supplemental Information** shows the open circuit voltage and the short-circuit current of the cell under variable irradiance conditions and different controlled temperature, along with the one of real operation conditions. The data in this figure is used to estimate the TPV cell temperature in operation. A linear dependence is found between the produced electric power and the cell temperature according to which cell temperature increases ~ 4 ºC per additional 100 mW$_{el}$ that are produced (panel b in **Figure S5)**. Despite this rate is very dependent on the specific cooling system and the kind of TPV cells that are used (e.g., the cells used in this experiment do not have a back surface reflector, and thus, need to dissipate large amounts of heat), this illustrates that cell cooling might be an issue at very high-power densities.

Finally, panel c in **Figure 13** shows the time evolution of the crucible temperature, as recorded by a calibrated pyrometer, and the projected TPV power density (dashed lines) calculated using the model mentioned above. The crucible contains 0.357 liters (3.19 kg) of copper in this case, which represents ~ 180 Wh of thermal energy in the form of latent heat. Different solidification processes are shown at different cooling rates, which are controlled by the electric power supplied to the heater from above. During the solidification, the temperature of the crucible keeps at an almost constant temperature in the range of 1050 – 1070 ºC, which is slightly lower than the melting point of copper (1080ºC) due to the temperature gradient in the crucible walls. Projected TPV power densities during the discharge are in the very narrow range of 500 – 550 mW/cm^2, almost independently of the cooling rate. The cooling rate, which is linked to the storage duration, barely affects the temperature gradient in this case due to the very high thermal conductivity of copper, although a slightly higher gradient is observed at the highest rate, as expected (**Figure 3**).

From the experiments shown in **Figure 13**, we can make some projections of the overall system performance. If the bottom part of the crucible (6 cm diameter) would be fully populated with TPV cells, the electricity produced by the system during the discharge would range from ~ 5.5 Wh to ~ 18 Wh for discharge durations between 0.37 and 1.22 hours (the two extreme values shown in **Figure 13**-c). This is a very small fraction (3 – 10 %) of the total latent heat contained in the PCM (180 Wh), which is attributed to the very high amount of heat loss existing in this lab prototype.

Remarkably, the heating electrodes are refrigerated and account for a large fraction of the heat loss, especially for short discharge times, where the input electricity to the electrodes is small and not enough to offset the heat loss. The steady state heat loss through the thermal insulation cover (25 cm of graphite fiber mat) at 1060 ºC crucible temperature is 156 W, as calculated using a CFD model and neglecting heat loss in the electrodes. This means that ~ 1.4 % of the stored latent heat is lost through the thermal insulation per minute. This very high value is attributed to i) the use of copper, which has a much lower energy density than Si or FeSiB; ii) the very small scale of the prototype, which is several orders of magnitude smaller than those considered in the previous sections; and iii) the relatively thin thermal insulation layer. Assuming a TPV conversion efficiency of 22 % (which has been reported for these cells [40]) and neglecting heat loss in the electrodes, the discharge efficiency (defined as the delivered electricity during the phase change divided by the total stored energy) and the discharge duration would be 6.6 % and 0.8 hours, respectively, which are in the range of values explored experimentally. If the heat loss would be drastically reduced to 3 %/day (i.e., passing from 156 W to 0.225 W of steady heat loss), the discharge efficiency and the storage duration would be increased to 21.9 % and 2.7 hours, respectively. Obviously, manufacturing such a well thermally insulated system is hardly attainable at these small scales, where the high surface-to-volume ratio leads to very high amount of heat loss. This again points to the relevance of scale in LHTPV systems.

5 Conclusions

LHTPV batteries that are based on Si (m.p. of 1414 ºC) or FeSiB (m.p. 1157 ºC) PCM can reach very low costs per energy capacity (< 10 €/kWh) at large scales, and thus, both are appealing solutions for long-duration storage applications. Their very high latent heat (1.2 MWh/m^3) enables very dense energy storage and small surface-to-energy ratios, ultimately resulting in relatively low thermal insulation requirements and low cost. The lower melting point of FeSiB further relaxes the thermal insulation requirements and enables lower costs per energy capacity, especially at smaller scales. Systems as small as 1 MWh are in principle possible using FeSiB PCM, whereas systems over 10 MWh are necessary for Si PCM to mitigate the impact of the more expensive thermal insulation system. The combination of high energy density and lower melting temperature of FeSiB makes this system especially appealing for long duration storage applications, where a low-cost and high-efficient thermal insulation is particularly important. Optimal heat losses, resulting from an optimal balance between cost and thermal insulation efficiency, are significantly lower in FeSiB

than in Si-based systems, offsetting the higher TPV conversion efficiencies attainable in Si-based systems. Besides, the long discharge duration ensures a minimal temperature gradient through the PCM during discharge, which is particularly important to ensure a low cost per power in such 'low' temperature FeSiB-based systems. On the contrary, the higher melting point of silicon enables a much higher TPV power density, ultimately resulting in a lower cost per discharge power capacity. Thus, Si-based systems are better suited for shorter duration applications, where the cost per power is more relevant. The cost per power capacity can be reduced in both kinds of systems by using very low bandgap TPV cells, like InGaAsSb (bandgap of 0.53 eV), or by designing the crucible to minimize the temperature gradients in the PCM during the discharge. In this work, a hollow cylindrical crucible unit has been considered, in which the temperature gradient is minimized by reducing the difference between crucible' inner and outer radius. This unavoidably brings a reduction in the amount of PCM per unit crucible, ultimately resulting in a lower energy density and a higher cost per energy capacity. Thus, a trade-off exists between cost per energy and power capacities that relies on the crucible design.

Besides of long duration storage applications, LHTPV brings some key advantages over Li-ion batteries for dispatchable cogeneration in fully electrified systems. The optimal solution takes advantage of the very low cost and high energy density of LHTPV to store the vast amounts of heat that otherwise should be stored at much lower energy densities in (e.g.) hot water tanks. As a result, the LHTPV-based solution has a slightly lower cost and a much higher energy density than a solution based on Li-ion batteries that relies on hot water tanks for heat storage. Like in long duration storage applications, large scales favor the use of LHTPV over Li-ion due to the lower cost per energy capacity. Large scales also enable lower cost of solar PV installations, which further benefit the use of a (cheaper) LHTPV system over a (more efficient) Li-ion battery in self-consumption applications.

An experimental test bed unit has been fabricated in the frame of the European Project AMADEUS that is intended to test materials and devices that will be eventually incorporated in an optimized LHTPV system. The first experimental results using copper PCM and GaSb TPV cells have been presented, illustrating the capabilities of this experimental setup to guide future developments.

6 Resource availability

6.1 Lead contact

Further information and requests for resources should be directed to and will be fulfilled by the lead contact, Alejandro Datas (a.datas@upm.es).

6.2 Materials availability

This study did not generate new unique materials.

6.3 Data and code availability

The data that support the findings of this study are available from the Lead author, upon reasonable request.

7 Acknowledgement

This work has been partially funded by the European FET-OPEN projects AMADEUS (grant agreement n. 737054) and NATHALIE (grant agreement n. 945858); by the projects Termocell (ENE2017-86683-R) and GeTPV (PID2020-115719RB-C22) from the National program Retos de la Sociedad funded by the Spanish Ministry of Economy, Industry and Competitivity; and by the project ANDREA from the "programa de apoyo a la realización de Proyectos de I+D para jóvenes investigadores 2019" funded by the Regional Government of Madrid. A. Ramos acknowledges the Serra Húnter Program from the Generalitat de Catalunya for her Serra Húnter Fellow post.

8 Author contributions

Conceptualization: A.D.; Funding acquisition: A.D.; Investigation: A.D, A.L.C, E.L., A.R,; Methodology: A.D, A.L.C, E.L., A.R,; Project administration: A.D; Resources: A.D, C.dC.; Software: A.D., A.L.C; Supervision: A.D.; Visualization: A.D.; Writing – original draft: A.D.; Writing – review & editing: A.D, A.L.C., E.L, A.R, C.dC.

9 Declaration of Interest

There are no competing interests

10 References

1. Datas, A. (2021). Ultra High Temperature Thermal Energy Storage for Dispatchable Power Generation. In Reference Module in Earth Systems and Environmental Sciences (Elsevier).

2. Datas, A., Ramos, A., and del Cañizo, C. (2019). Techno-economic analysis of solar PV power-to-heat-to-power storage and trigeneration in the residential sector. Appl. Energy *256*, 113935.

3. Datas, A., Ramos, A., Marti, A., del Canizo, C., and Luque, A. (2016). Ultra high temperature latent heat energy storage and thermophotovoltaic energy conversion. Energy *107*, 542–549.

4. Okazaki, T. (2020). Electric thermal energy storage and advantage of rotating heater having synchronous inertia. Renew. Energy *151*, 563–574.

5. Amy, C., Seyf, H.R., Steiner, M.A., Friedman, D.J., and Henry, A. (2018). Thermal energy grid storage using multi-junction photovoltaics. Energy Environ. Sci., 334–343.

6. Burger, T., Sempere, C., Roy-Layinde, B., and Lenert, A. (2020). Present Efficiencies and Future Opportunities in Thermophotovoltaics. Joule.

7. Datas, A., and Vaillon, R. (2021). Chapter 11 - Thermophotovoltaic energy conversion. In Ultra-High Temperature Thermal Energy Storage, Transfer and Conversion Woodhead Publishing Series in Energy., A. Datas, ed. (Woodhead Publishing), pp. 285–308.

8. Safarian, J., and Tangstad, M. (2021). Chapter 4 - Phase change materials for high-temperature operation. In Ultra-High Temperature Thermal Energy Storage, Transfer and Conversion Woodhead Publishing Series in Energy., A. Datas, ed. (Woodhead Publishing), pp. 85–111.

9. Albertus, P., Manser, J.S., and Litzelman, S. (2020). Long-Duration Electricity Storage Applications, Economics, and Technologies. Joule *4*, 21–32.

10. Mongird, K., Viswanathan, V., Alam, J., Vartanian, C., and Sprenkle, V. (2020). 2020 Grid Energy Storage Technology Cost and Performance Assessment (U.S. Department of Energy).

11. Laughlin, R.B. (2017). Pumped thermal grid storage with heat exchange. J. Renew. Sustain. Energy *9*, 044103.

12. Datas, A. ed. (2021). Ultra-High Temperature Thermal Energy Storage, Transfer and Conversion (Woodhead Publishing).

13. Parham, J., Vrettos, P., and Levinson, N. (2021). Chapter 13 - Commercialisation of ultra-high temperature energy storage applications: the 1414 Degrees approach. In Ultra-High Temperature Thermal Energy Storage, Transfer and Conversion Woodhead Publishing Series in Energy., A. Datas, ed. (Woodhead Publishing), pp. 331–346.

14. Rhim, W.-K., and Ohsaka, K. (2000). Thermophysical properties measurement of molten silicon by high-temperature electrostatic levitator: density, volume expansion, specific heat capacity, emissivity, surface tension and viscosity. J. Cryst. Growth *208*, 313–321.

15. Gilpin, M.R. (2015). High temperature latent heat thermal energy storage to augment solar thermal propulsion for microsatellites.

16. Jiao, J., Grorud, B., Sindland, C., Safarian, J., Tang, K., Sellevoll, K., and Tangstad, M. (2019). The Use of Eutectic Fe-Si-B Alloy as a Phase Change Material in Thermal Energy Storage Systems. Materials *12*.

17. Lang, S., Drück, H., and Bestenlehner, D. (2021). Chapter 8 - Ultrahigh temperature thermal insulation. In Ultra-High Temperature Thermal Energy Storage, Transfer and Conversion Woodhead Publishing Series in Energy., A. Datas, ed. (Woodhead Publishing), pp. 201–219.

18. Forsberg, C.W., Stack, D.C., Curtis, D., Haratyk, G., and Sepulveda, N.A. (2017). Converting excess low-price electricity into high-temperature stored heat for industry and high-value electricity production. Electr. J. *30*, 42–52.

19. Mishra, R.R., and Sharma, A.K. (2016). Microwave–material interaction phenomena: Heating mechanisms, challenges and opportunities in material processing. Compos. Part Appl. Sci. Manuf. *81*, 78–97.

20. Edgerley, C.J., Smith, L., and Wilford, C.F. (1988). Electric metal melting-a review. Power Eng. J. *2*, 83–92.

21. Datas, A., Zeneli, M., del Cañizo, C., Malgarinos, I., Nikolopoulos, A., Nikolopoulos, N., Karellas, S., and Martí, A. (2018). Molten silicon storage of concentrated solar power with integrated thermophotovoltaic energy conversion. In AIP Conference Proceedings, p. 090005.

22. Zaversky, F., García-Barberena, J., Sánchez, M., and Astrain, D. (2013). Transient molten salt two-tank thermal storage modeling for CSP performance simulations. Sol. Energy *93*, 294–311.

23. Schulte-Fischedick, J., Tamme, R., and Herrmann, U. (2009). CFD Analysis of the Cool Down Behaviour of Molten Salt Thermal Storage Systems. In (American Society of Mechanical Engineers Digital Collection), pp. 515–524.

24. Stack, D.C. (2017). Conceptual design and performance characteristics of firebrick resistance-heated energy storage for industrial heat supply and variable electricity production.

25. Stack, D.C., Curtis, D., and Forsberg, C. (2019). Performance of firebrick resistance-heated energy storage for industrial heat applications and round-trip electricity storage. Appl. Energy *242*, 782–796.

26. Datas, A., and Marti, A. (2017). Thermophotovoltaic energy in space applications: Review and future potential. Sol. Energy Mater. Sol. Cells *161*, 285–296.

27. Omair, Z., Scranton, G., Pazos-Outón, L.M., Xiao, T.P., Steiner, M.A., Ganapati, V., Peterson, P.F., Holzrichter, J., Atwater, H., and Yablonovitch, E. (2019). Ultraefficient thermophotovoltaic power conversion by band-edge spectral filtering. Proc. Natl. Acad. Sci. *116*, 15356–15361.

28. Horowitz, K.A.W., Woodhouse, M., Lee, H., and Smestad, G.P. (2015). A bottom-up cost analysis of a high concentration PV module. AIP Conf. Proc. *1679*, 100001.

29. Palfinger, G. nther, Bitnar, B., Durisch, W., Mayor, J.-C., tzmacher, D.G., and Gobrecht, J. (2003). Cost estimate of electricity produced by TPV. Semicond. Sci. Technol. *18*, S254–S261.

30. Datas, A. (2015). Optimum semiconductor bandgaps in single junction and multijunction thermophotovoltaic converters. Sol. Energy Mater. Sol. Cells *134*, 275–290.

31. Fan, D., Burger, T., McSherry, S., Lee, B., Lenert, A., and Forrest, S.R. (2020). Near-perfect photon utilization in an air-bridge thermophotovoltaic cell. Nature, 1–5.

32. Schmidt, O., Melchior, S., Hawkes, A., and Staffell, I. (2019). Projecting the Future Levelized Cost of Electricity Storage Technologies. Joule *3*, 81–100.

33. EnergyPlus™.

34. PVsyst Software http://www.pvsyst.com/en/software.

35. Datas, A., Ramos, A., and del Cañizo, C. (2019). Techno-economic analysis of solar PV power-to-heat-to-power storage and trigeneration in the residential sector. Appl. Energy *256*, 113935.

36. Datas, A., López, E., Ramos, A., Nikolopoulos, N., Nikolopoulos, A., Zeneli, M., Sobczak, N., Polkowski, W., Tangstad, M., Safarian, J., et al. (2020). Ultra-high temperature energy storage and conversion: A review of the AMADEUS project results. AIP Conf. Proc. *2303*, 190008.

37. Datas, A., Chubb, D.L., and Veeraragavan, A. (2013). Steady state analysis of a storage integrated solar thermophotovoltaic (SISTPV) system. Sol. Energy *96*, 33–45.

38. Veeraragavan, A., Montgomery, L., and Datas, A. (2014). Night time performance of a storage integrated solar thermophotovoltaic (SISTPV) system. Sol. Energy *108*, 377–389.

39. Chubb, D.L., Good, B.S., and Lowe, R.A. (1995). Solar thermophotovoltaic (STPV) system with thermal energy storage. In, pp. 181–198.

40. Fraas, L.M., Samaras, J.E., Huang, H.X., Minkin, L., Avery, J.E., and Daniels, W.E. TPV generators using the radiant tube burner configuration. In Proceedings of the, 17 (Europa PVSEC), pp. 22–26.

41. Amy, C., Kelsall, C.C., LaPotin, A., Pishahang, M., and Henry, A. (2021). Chapter 3 - Ultrahigh temperature sensible heat storage and heat transfer fluids. In Ultra-High Temperature Thermal Energy Storage, Transfer and Conversion Woodhead Publishing Series in Energy., A. Datas, ed. (Woodhead Publishing), pp. 57–84.

11 Figure legends and Tables

Figure 1. Diagram illustrating the key components of a LHTPV battery with one input (electricity) and two possible outputs (heat and electricity).

Figure 2. A LHTPV system based on the hollow cylindrical crucible units described in [3].

Figure 3. Emitter temperature during the discharge of different LHTPV systems as a function of discharge duration (i.e., average energy-to- (output thermal) power ratio). Solid lines represent the average emitter temperature during discharge and colored bands represent the full range of emitter temperatures during the discharge. The discharge time is modified through the variation of the effective TPV cell area. Smaller TPV generators produce smaller heat flux, and thus, smaller temperature gradients over the discharge. In this simulation, a container with 4 cm thick SiC walls (L_{cont}= 4 cm), emitter enclosure of 10 cm diameter (R_{cav}= 5 cm) and different external radius (R_{cont} = 34 cm for red curves and R_{cont} = 19 cm for blue curves) is considered. Results are shown for both Si (melting point of 1414ºC) and FeSiB (melting point of 1157ºC) PCMs. The minimum discharge time shown for each configuration corresponds to the heat flux conditions of an emitter cavity fully populated with InGaAsSb cells (0.53 eV bandgap) with 95% back-surface reflectivity. The top view of the crucibles is illustrated next to each corresponding curve for the case of pure Si PCM.

Figure 4. Panels (a) and (b) show the cost per energy capacity (CPE) in €/kWh of complete LHTPV systems of 1 MWh (panel a) and 100 MWh (panel b) capacity as a function of the melting temperature and the latent heat of the phase change material (PCM). The height of the crucibles is set to H = 0.5 m (panel a) and H= 1.5 m (panel b), and the cost per volume of the PCM (CPV) is set to 3.29 €/l to illustrate the case of using Si or FeSiB PCM. Panels (c) and (d) show the CPE and the energy density, respectively, as a function of energy storage capacity of a LHTPV system that uses either Fe, Si or FeSiB PCMs and are comprised of NxN crucibles, of a height (H) that is varied from 1.5 m to 0.5 m, determining the lower and upper bounds of each colored band, respectively. Panels (e) and (f) show the CPE and the energy density, respectively, as a function of the self-discharge duration for a 1 GWh LHTPV system using the same PCMs. In this case, the lower and upper bounds of the colored bands represent crucible heights ranging from 2 to 5 m, respectively. In all panels, the thermal insulation cover is composed of two layers, the outermost being fumed silica board (2.5 €/l) and the innermost alumina fiber mat (7 €/l) [17]. The thickness of these two layers is calculated to get a maximum temperature for the silica board of 1000 ºC and the desired amount of heat loss in each case. The PCM container is assumed to be made of silicon carbide, and the thermophysical and cost data of the materials are taken from **Table 1**. Otherwise indicated, heat loss (self-discharge duration) is set to 5 %/day (20 days or 480 hours) and the crucibles have L_{cont} = 4 cm, R_{cont} = 34 cm, and R_{cav} = 5 cm. The number of crucibles is set to provide the required energy capacity in each case.

Figure 5. TPV conversion efficiency (panel a) and cost per power (panel b) as a function of the emitter temperature for InGaAs (bandgap 0.75 eV) and InGaAsSb (bandgap 0.53 eV) TPV cells. The cells have been modeled using a detailed balance approach [26] assuming an internal luminescence efficiency of 84% (reported for InGaAs TPV cells [27]). In panel a, sub-bandgap reflectivities in the range of 90 to 98 % are represented in each band. The ideal case of TPV cells with an internal luminescence efficiency of 100% is also shown as a

reference. In panel b, bands represent different costs per unit of area in the range of 1 to 3 €/cm^2. In both panels, dashed lines represent the case of cells with a series resistance of 10 mΩ (cell area is 1 cm^2). In all simulations, the emitter emissivity is set to 0.9 and the TPV cells operate at 80 ºC.

Figure 6. Cost per output power capacity (CPP_{out}) as a function of the discharge duration for LHTPV systems based on Si (panel a) and FeSiB (panel b) PCMs, using InGaAs (yellow) and InGaAsSb (red) TPV generators, and containers with R_{cont} = 34 cm (solid lines) and R_{cont} = 19 cm (dashed lines). Colored regions represent the uncertainty assumed in this work for the TPV generator cost of 1 – 3 €/cm^2. All simulations assume a TPV generator with overall sub-bandgap reflectivity of 95 %.

Figure 7. Cost per energy capacity (CPE) and cost per power capacity (CPP) of a LHTPV system with 100 MWh of energy capacity, 50 h of discharge time, and 1000 h of self-discharge duration (heat loss of 2.4 %/day). Each point represents a different system configuration that uses Si or FeSiB PCMs, InGaAs or InGaAsSb TPV cells, and containers with R_{cont} = 34 or 19 cm (indicated as numbers near each point in the graph). All LHTPV systems have L_{cont} = 4 cm and R_{cav} = 5 cm. CPE errors bar indicate systems with H = 1 m (upper bound) and H = 2 m (lower bound). CPP error bars indicate TPV generator cost of 3 €/cm^2 (upper bound) and 1 €/cm^2 (lower bound). The case of Li-ion batteries, lead-acid, and vanadium redox flow batteries (VRFB) [10], as well as pumped hydroelectric (PHS), compressed air storage (CAES) and Hydrogen [32] are also plotted as a reference.

Figure 8. Relative difference in LCOS between LHTPV and Li-ion batteries of 100 MWh capacity as a function of the TPV efficiency, the heat loss (panels a-d) and the storage duration (e-f) for LHTPV systems based on Si (panels a, c, and e) and FeSiB (panels b, d and f) PCMs. In panels e and f, the heat loss is optimized (i.e., set to the value that minimizes the LCOS). In all the cases, CPP and CPE for Li-ion batteries are set to 52.5 €/kW and 87 €/kWh, respectively, which represents the best-case scenario in Figure 7. CPP and CPE for LHTPV batteries assume the most favorable case in Figure 6 (InGaAsSb TPV cells at 1 €/cm2), Rcont = 34 cm, Lcont = 4 cm, Rcav = 5 cm, and an optimized crucible height (i.e., the one that minimizes CPE). LCOS is calculated assuming an input cost of electricity of 1 c€/kWh, a discount rate of 7 %, and a system lifetime is 25 years, and assuming a symmetric cycling (charging time equals discharging time, i.e., $t_c = t_d$).

Figure 9. Panels a - d show the breakeven TPV efficiency as a function of the storage duration and the storage capacity for Si- (panels a and c) and FeSiB-based (panels b and d) LHTPV systems using high-cost (3 €/cm^2) InGaAs (panels c and d) and low cost (1 €/cm^2) InGaAsSb (panels a and b) TPV cells. Panels e and f show the relative difference in breakeven TPV efficiency between LHTPV systems based on Si and FeSiB PCMs that use low-cost (1 €/cm^2) InGaAsSb (panel e) and high-cost (3 €/cm^2) InGaAs (panel f) TPV cells. Breakeven efficiency is defined as the one that results in an identical LCOS for LHTPV and Li-ion batteries.

In all the cases, CPP and CPE for Li-ion batteries are set to 52.5 €/kW and 87 €/kWh, respectively, which represents the best-case scenario in **Figure 7**. The CPE for LHTPV batteries is calculated assuming R_{cont} = 34 cm, L_{cont} = 4 cm, R_{cav} = 5 cm, and an optimized crucible height (i.e., the one that minimizes CPE). LCOS is calculated assuming an input cost of electricity of 1 c€/kWh, a discount rate of 7 %, and a system lifetime is 25 years, and assuming a symmetric cycling (charging time equals discharging time, i.e., $t_c = t_d$).

Figure 10. Complete system configurations for energy storage and cogeneration in a fully electrified building that uses Li-ion (panel a) and LHTPV (panel b) batteries. The electric demand includes air conditioning (AC).

Figure 11. Panels (a) and (b) show the levelized cost of energy (in €/kWh) and the total energy density of the two system configurations illustrated in **Figure 10** as a function of the yearly energy demand (heat and electricity). For Li-ion batteries, each colored band represents the value obtained within the margin of confidence for CPP and CPE, which are indicated in **Table 3**. For LHTPV systems, each colored band represents the upper and lower bounds of CPP, which are taken from **Figure 6**, and thus, depend on the cost of TPV (1 – 3 €/W) and the discharge duration at nominal power conditions. The LHTPV system has R_{cont} = 34 cm, L_{cont} = 4 cm, R_{cav} = 5 cm. The CPE for LHTPV is determined by the heat loss (%/day) and the height of the crucibles, both being optimized parameters. Panel (c) shows the levelized cost of energy for the best-case scenarios of a LHTPV system (using FeSiB PCM and InGaAsSb TPV cells) and a Li-ion battery with different assumptions of the cost of the PV installation, ranging from 600 €/kW to 2000 €/kW. Both systems with a fixed (1.5 m) and an optimized crucible height are shown. In all cases, the TPV conversion efficiency is assumed to be 35 % and 40 % for the systems based on FeSiB and Si PCM, respectively. Otherwise indicated, **Table 3** describes the parameters that have been set to a constant value or that have been optimized in these simulations. The optimal parameters corresponding to the results shown in panels a and b are shown in **Figure S4** of the **Supplemental Information**.

Figure 12. Levelized cost of energy (LCOE, in €/kWh) as a function of TPV conversion efficiency for a cogeneration solution (**Figure 10**) that uses a LHTPV battery that is based on InGaAsSb TPV cells and uses either Si (yellow curves) and FeSiB (red curves) PCMs. The LCOE for the case of Li-ion batteries is shown as a reference. The systems have been optimized for a yearly annual demand of 2 GWh/year (i.e., an average daily consumption 1.1 MWh of electricity and 4.4 MWh of heat) and the sizing of each element of the system (PV installation and stores capacities) along with other LHTPV parameters (heat loss and crucible height) have been optimized to obtain the minimum LCOE. The optimum storage capacity of the LHTPV system ranges from 12 – 15 MWh (for Si systems) to 13 – 15 MWh (for FeSiB systems) and the optimal heat loss from ~ 4 %/day (for Si systems) to ~ 2.5 %/day (for FeSiB systems), independently of the TPV efficiency. The optimal size of the PV installation is ~ 2 MW, independently of the type of LHTPV system and TPV conversion efficiency.

Figure 13. LHTPV lab prototype characterization results: (a) Short-circuit current produced by the GaSb TPV cell as a function of the crucible temperature. Pictures of the TPV cell in operation (irradiated by the bottom part of the incandescent crucible) and a few examples of the I-V curves of the TPV cells under the different irradiance conditions are shown in the inset. (b) Experimental and calculated TPV power density as a function of the crucible temperature. Calculated values are obtained from a detailed balance TPV model that is explained elsewhere [26]. The worst-case scenario for the calculated power density (1) assumes a crucible (emitter) emissivity of 0.81, a cell bandgap of 0.726 eV (GaSb), an internal electroluminescent efficiency (η_{int}) of 1 %, a back surface reflector (BSR) reflectivity of 10 % and series resistance (R_s) of 50 mΩ. Different scenarios (2 – 6) assume incremental improvements which are indicated in the inset. InGaAsSb cells have a

bandgap of 0.53 eV. (d) The crucible temperature and the projected TPV power density as a function of time during the cool down of the crucible. Results for an empty crucible and a crucible filled with 3.19 kg of copper are shown. Different cooling rates are obtained varying the supplied power to the upper part of the crucible.

Table 1. Thermophysical properties of selected materials used for TES in LHTPV systems.

Material	Density (g/cm^3)	Specific heat (J/gK)	Latent Heat (J/g)	Thermal conductivity ($Wm^{-1}K^{-1}$) [(i)]	Melting / Maximum Temperature (ºC)	CPV (€/l)	Refs
Si	2.33	0.98	1800	29 (solid) 60 (liquid)	1414	3.29	[1,16,41]
Fe	7.86	0.72	247	36 (solid) 40 (liquid)	1538	0.84	[1,16,41]
Fe-26Si-9B	5.39	0.95	777	30 (solid) 60 (liquid)	1157	3.29[(ii)]	[16]
SiC	3.21	1.26	-	-	2827	3.21	[41]
Alumina fiber mat[(iii)]			-	0.26	1650 (max)	7	[17]
Fumed silica board[(iv)]			-	0.034	1000 (max)	2.5	[17]

[(i)] Data provided at approximately 1000 ºC
[(ii)] The cost per volume of FeSiB is assumed to be identical to that of silicon.
[(iii)] Alumina mat by Zircar Ceramics (USA)
[(iv)] WDS Ultra by Morgan Advanced Materials (UK)

Table 2. Techno-economic assumptions for the components shown in **Figure 10**. Ambient temperature is assumed 25 ºC.

Component	***Parameter***	***Value***
PV installation	Cost per power capacity	900 €/kW
	Nominal PV power installed	**Optimized** (kW)
Hot water storage	Cost per energy capacity	30 €/ kWh
	Energy capacity	**Optimized (**kWh)
	Heat loss	0.1 $W \cdot K^{-1} \cdot dm^{-3/2}$
	Electric heater efficiency	100 %
	Temperature of storage	60 ºC
LHTPV battery	Height of the crucibles	**Optimized** (m)
	Cost per energy capacity	Calculated for each size and heat loss (€/kWh)
	Energy capacity	**Optimized** (kWh)
	Cost per input power capacity	20 €/kW
	Input power capacity	**Optimized** (in (kW)
	Cost per output power capacity	Calculated for each storage duration (€/kW)
	Output power capacity	**Optimized** (kW)
	Self-discharge (heat loss)	**Optimized** (%/day)
Li-ion battery	Cost per energy capacity	87 – 145 €/kWh
	Energy capacity	**Optimized** (kWh)
	Cost per input power capacity	52.5 – 60.8 €/kW
	Input power capacity	**Optimized** (kW)
	Cost per output power capacity	0 €/kW
	Output power capacity	Equal to the input power capacity
	Self-discharge	0 %/day
	Round-trip efficiency	90 %
Electric grid	Cost of grid electricity	0.17 €/kWh [35]
	Cost of grid power capacity	50 €/kW [35]
	Price of electricity injected to the grid	0 €/kWh
Other economic variables	Weighted Average Cost of Capital	4 % [35]
	Inflation	2 % [35]
	Lifetime of all technologies	25 years

Figure 1

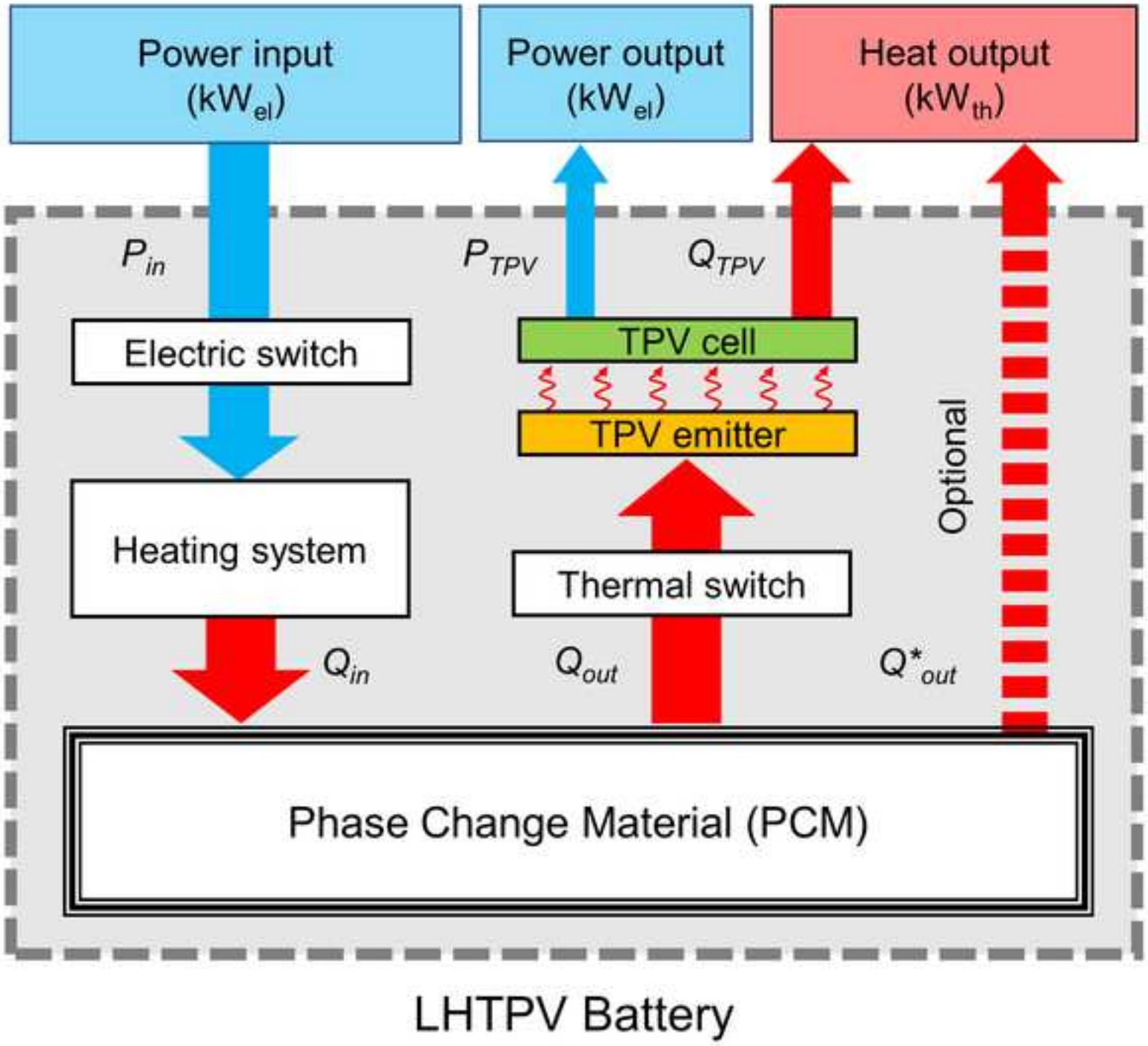

Figure 2

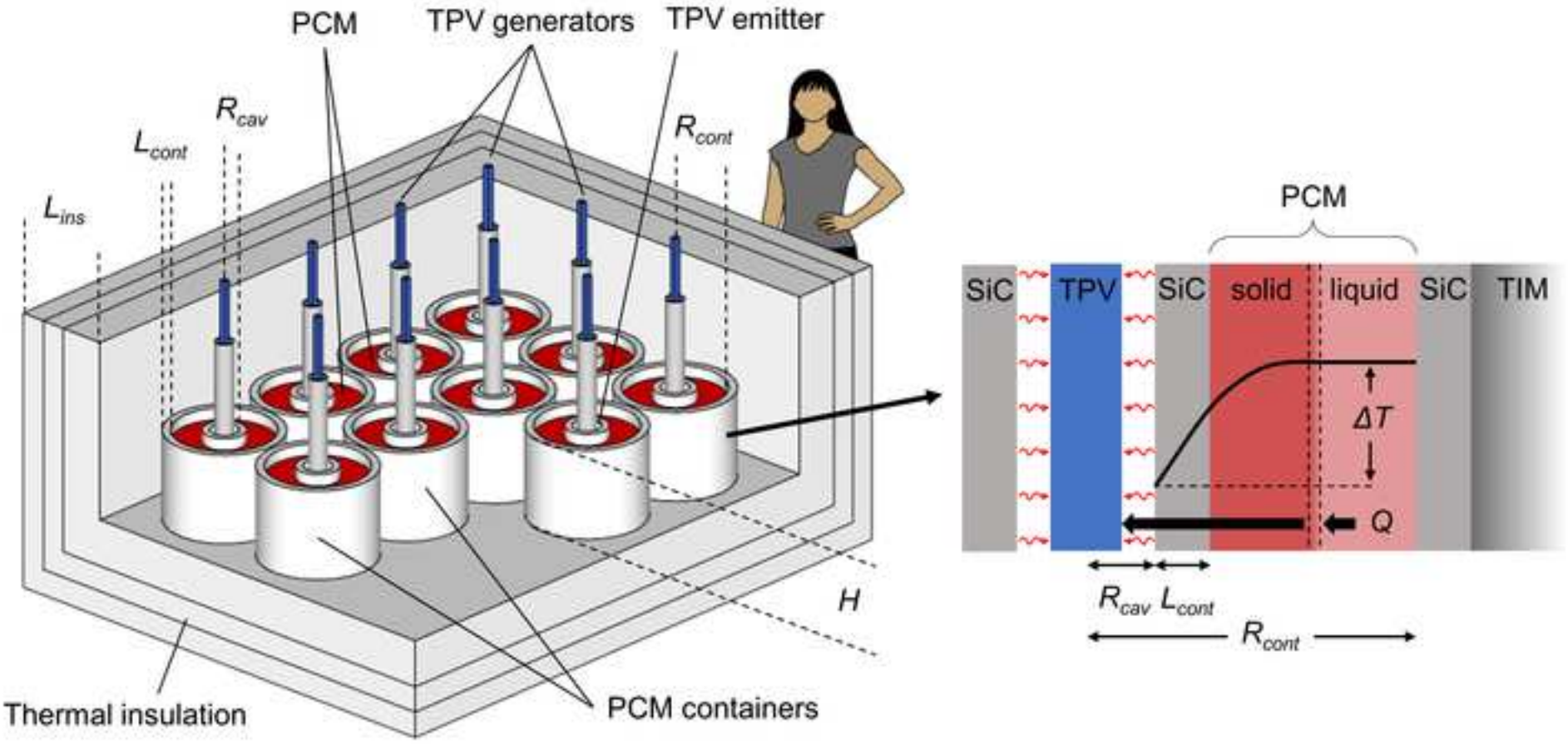

Figure 3

Click here to access/download;Figure;Fig3_new.tif

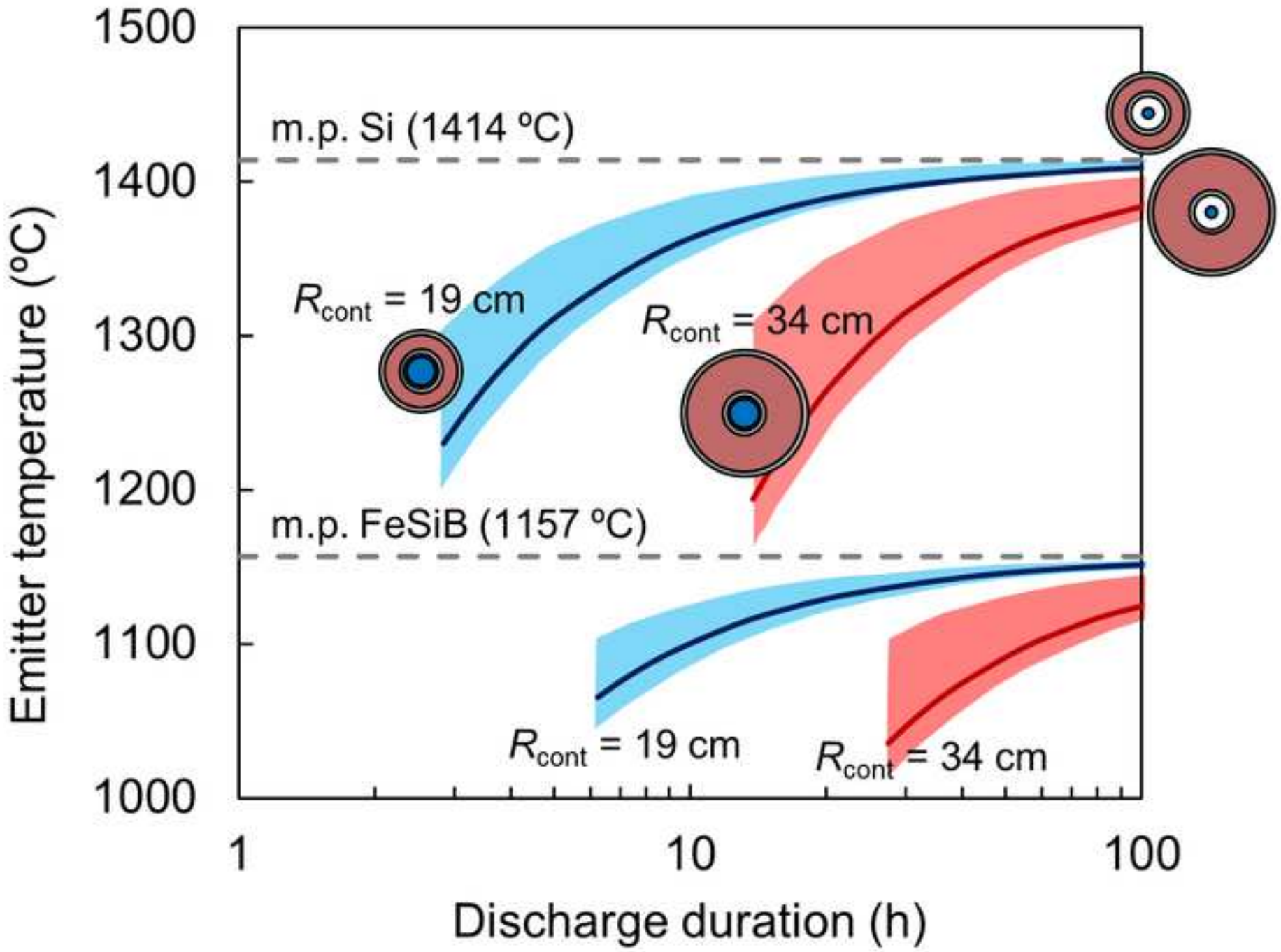

Figure 4

Click here to access/download;Figure;Fig4_new.tif

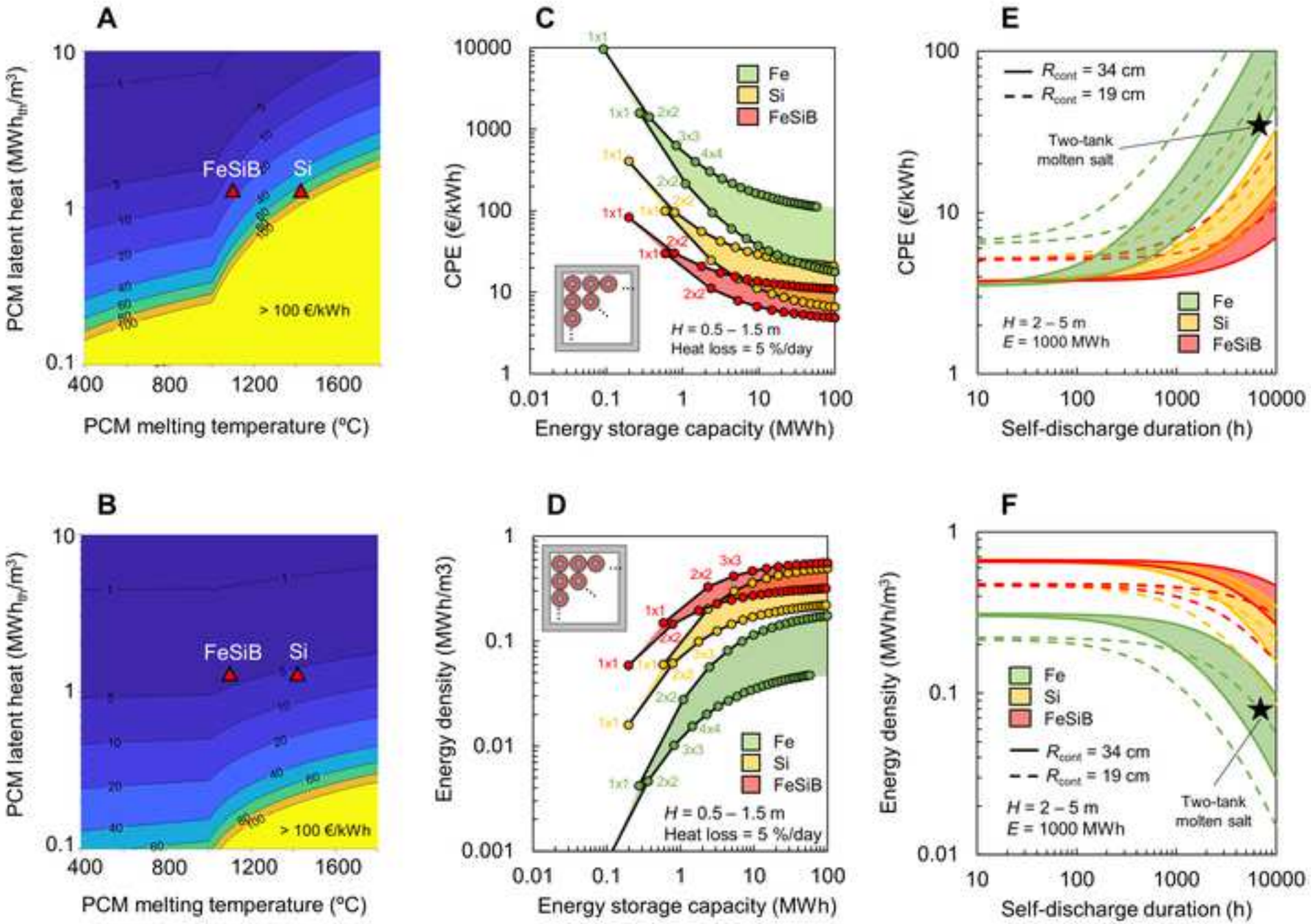

Figure 5

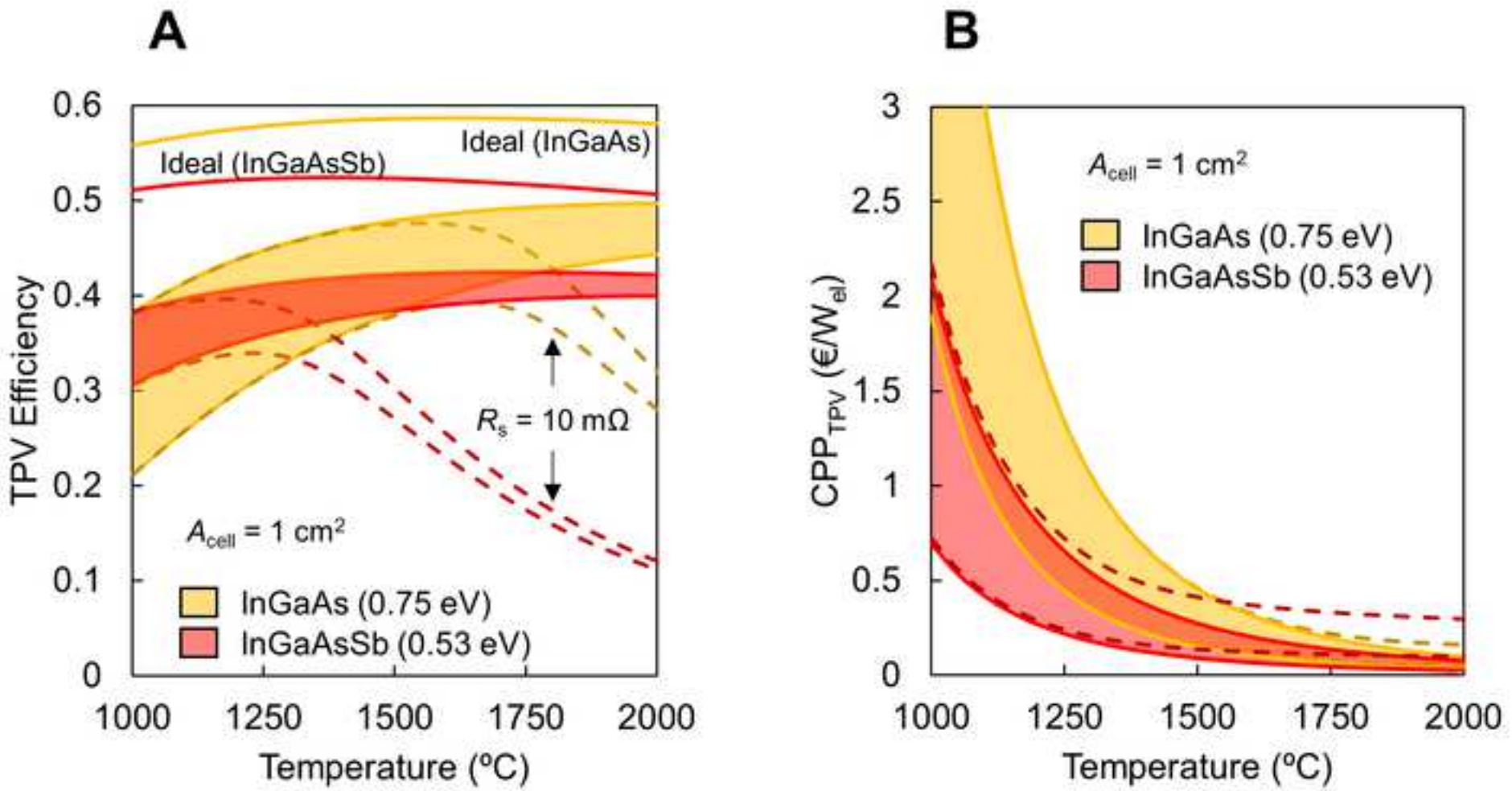

Figure 6

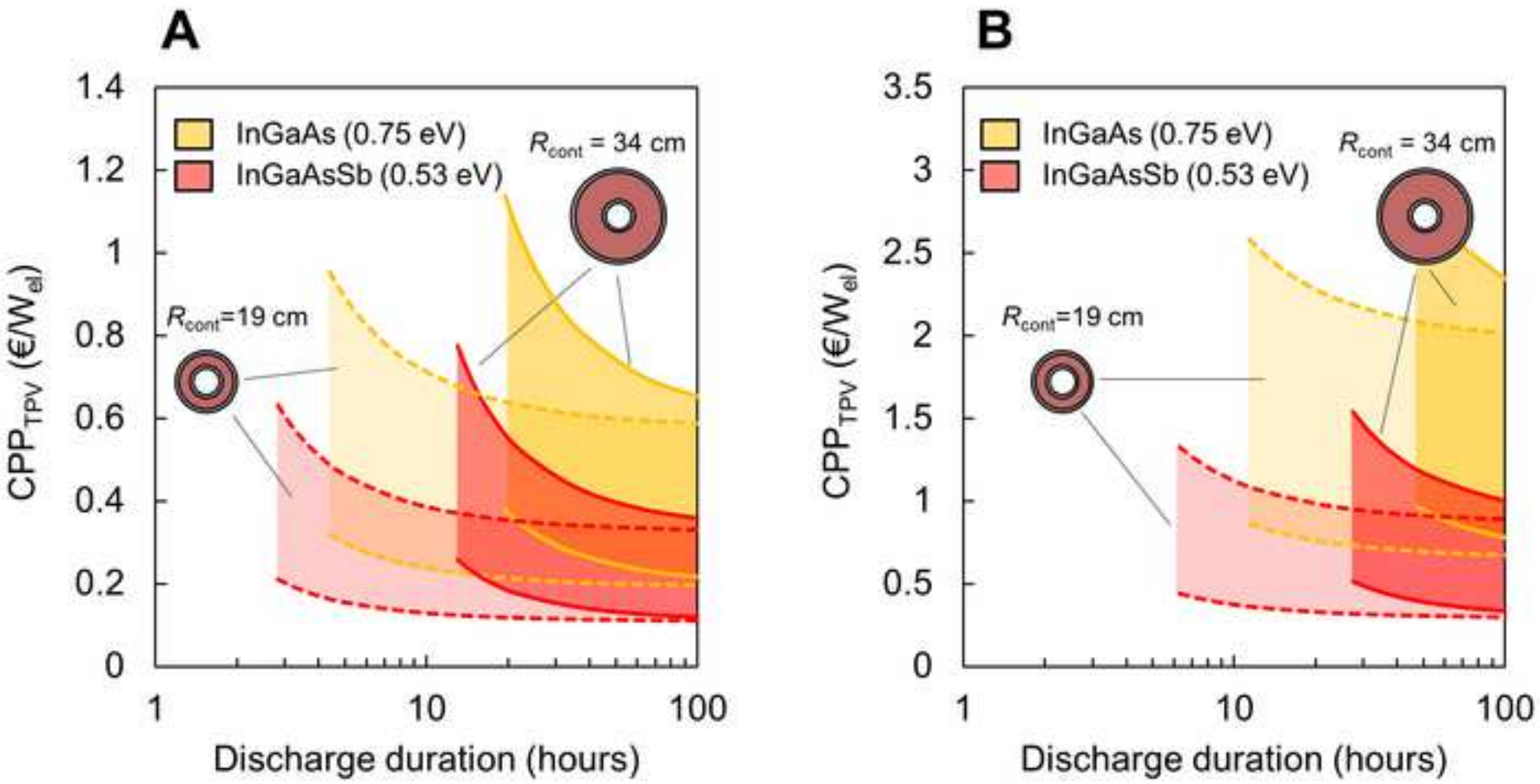

Figure 7

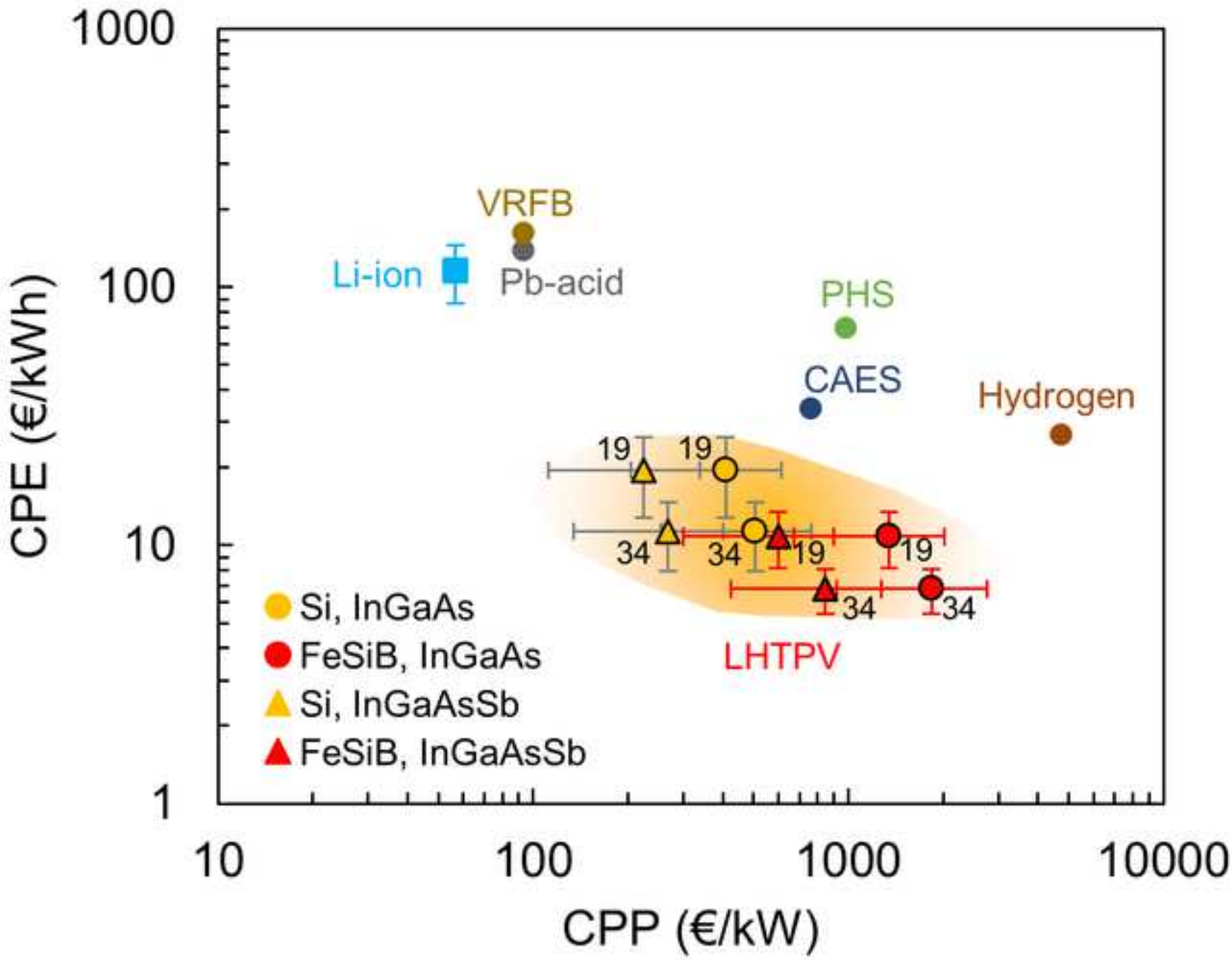

Figure 8

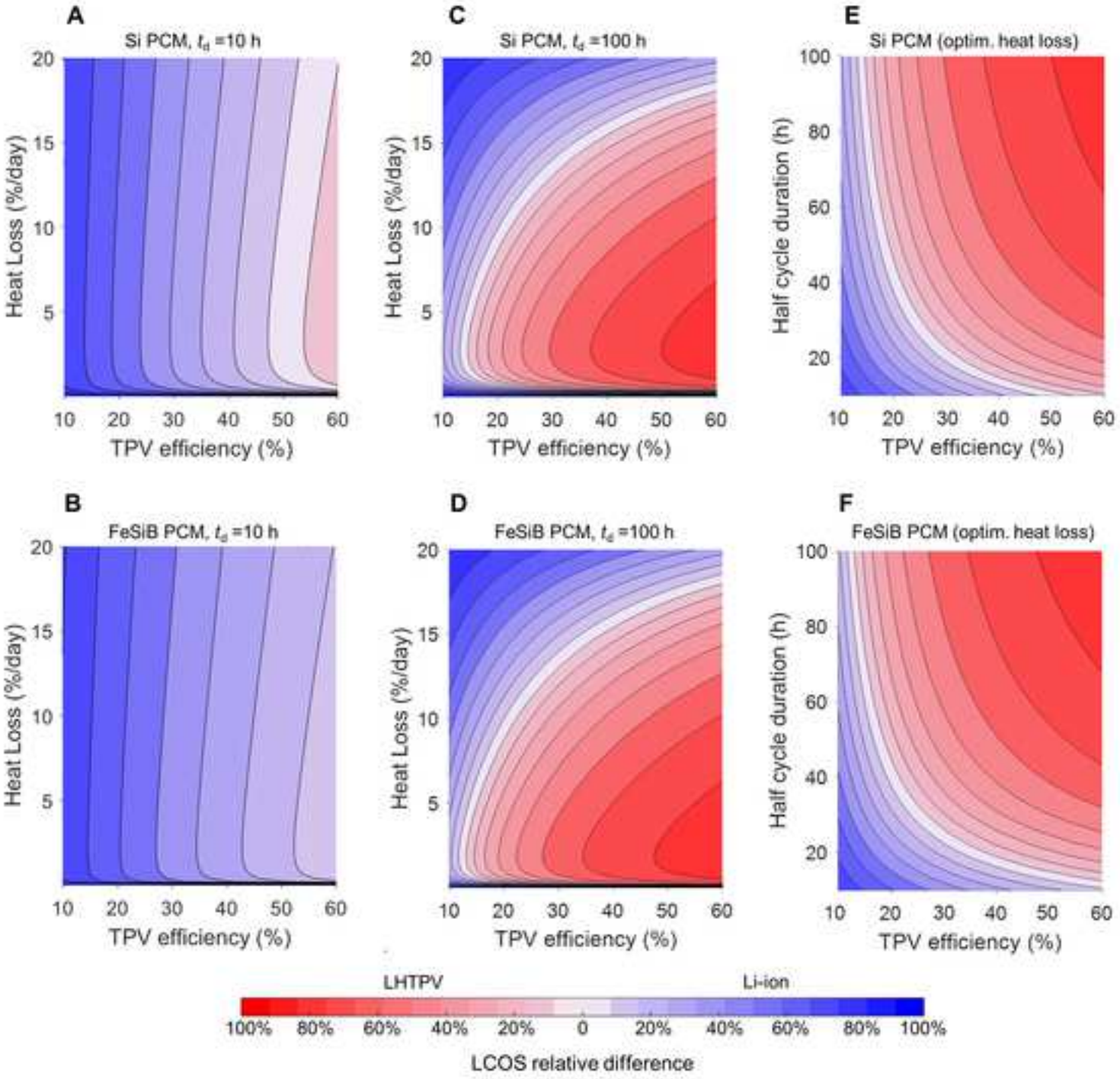

Figure 9

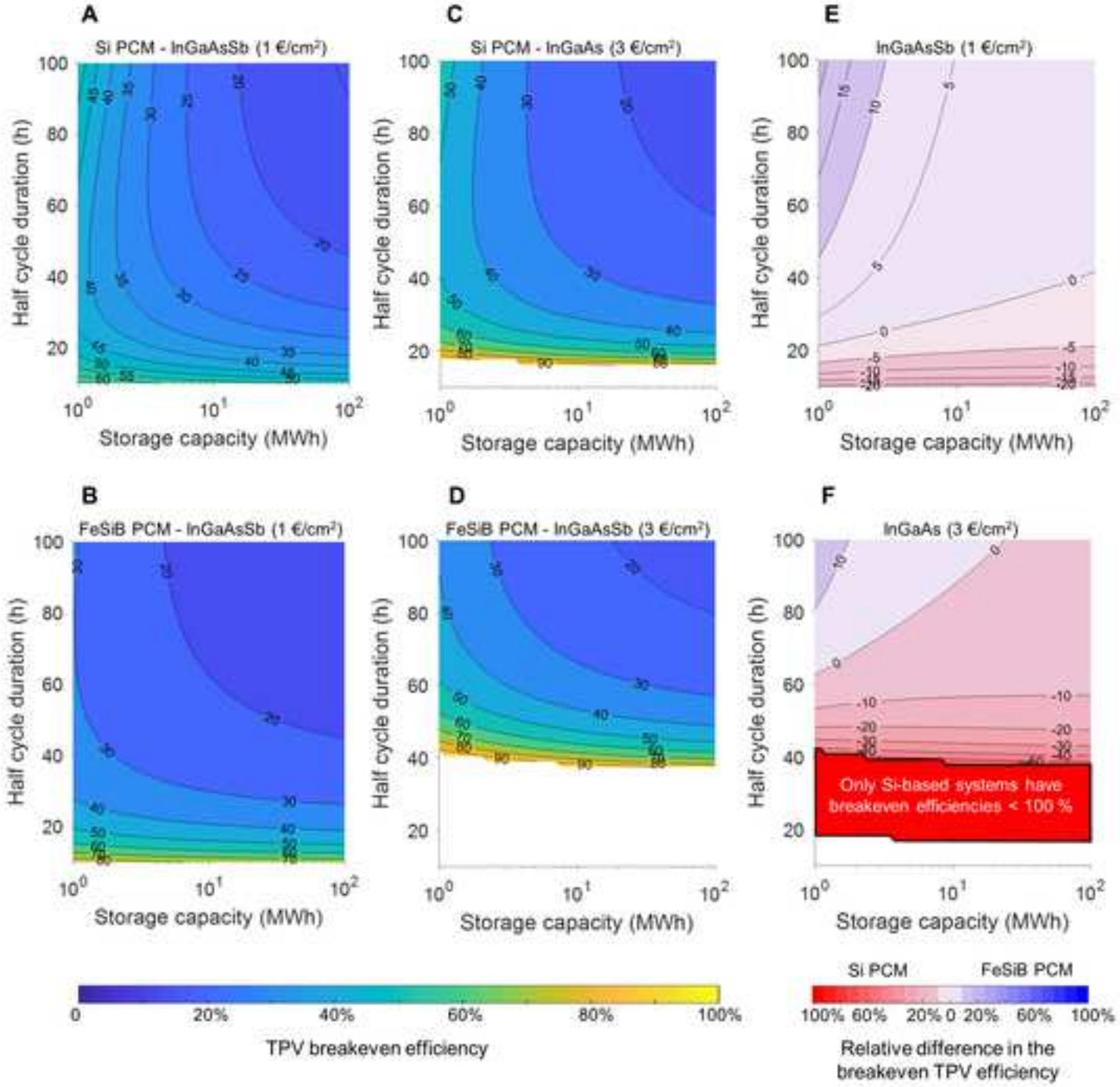

Figure 10

Click here to access/download;Figure;Fig10.tif

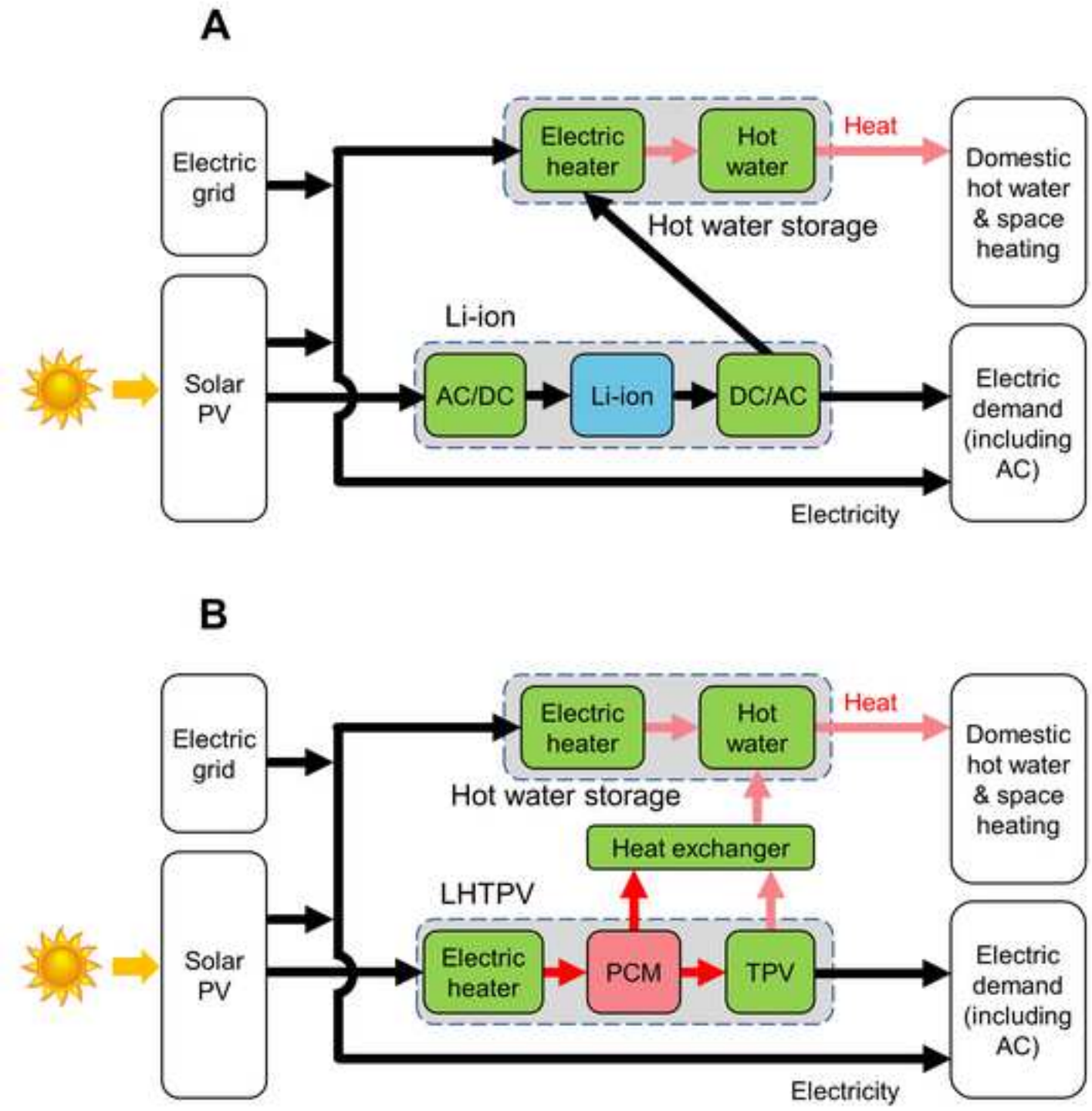

Figure 11

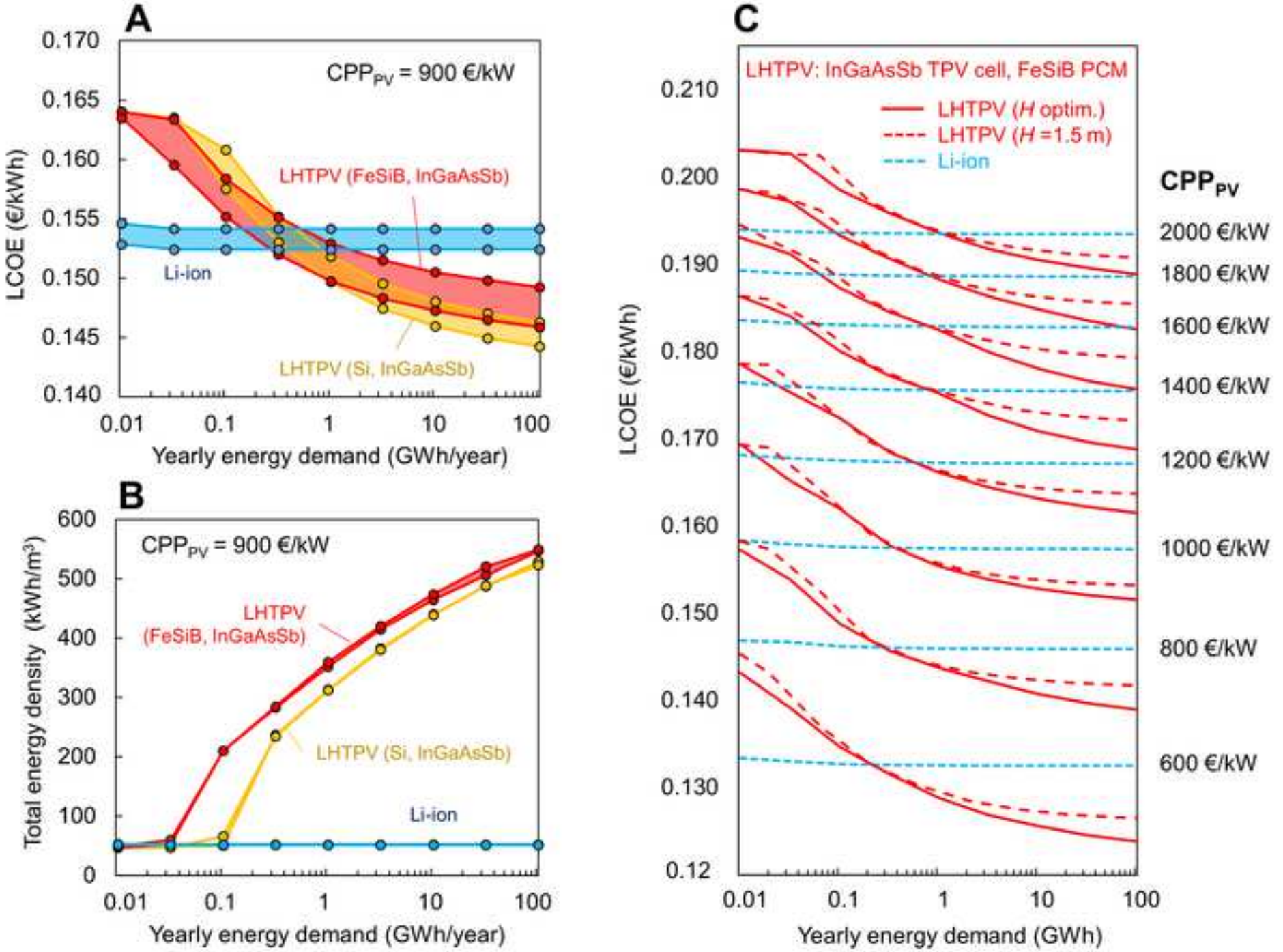

Figure 12

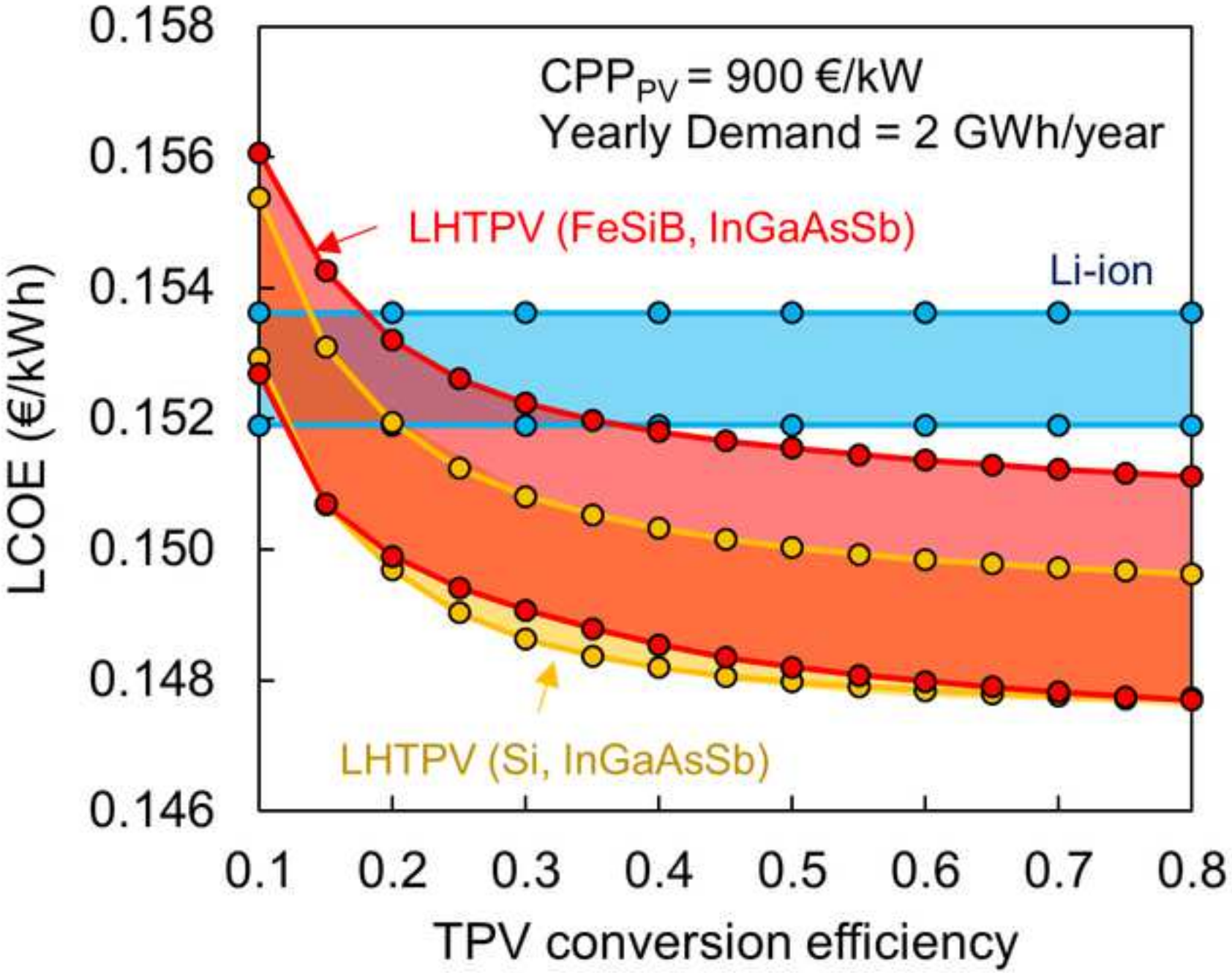

Figure 13

Click here to access/download;Figure;Fig13_new.tif